CASL-U-2015-1016-000

A DOE Energy Innovation Hub

L2.FMC.P11.01 Demonstrate 3D PCI analysis with BISON-CASL for PCI fuel failure in a commercial power reactor

Nathan Capps[1], Wenfeng Liu[2], Robert Montgomery[3], Martin Pytel[4], Joe Rashid[2], Ben Spencer[5], Dion Sunderland[3], Rich Williamson[5], and Brian D. Wirth[1]

1. University of Tennessee, Knoxville
2. Anatech Corp.
3. Pacific Northwest National Laboratory
4. Electric Power Research Institute
5. Idaho National Laboratory

September 30, 2015

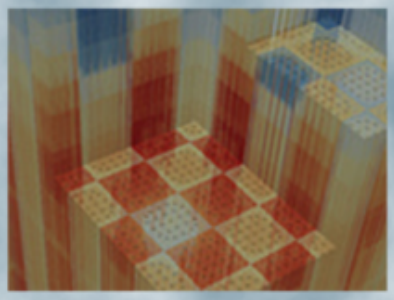

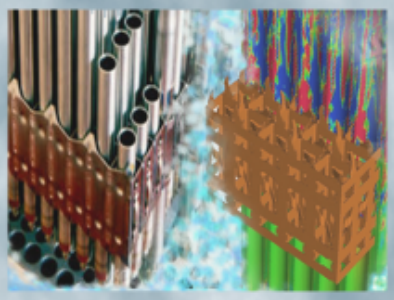

U.S. DEPARTMENT OF ENERGY | Nuclear Energy

CASL-U-2015-1016-000

Please complete sections appropriate for this record.

REVISION LOG

Revision	Date	Affected Pages	Revision Description
0		All	Initial Release

Document pages that are:

Export Controlled _____

IP/Proprietary/NDA Controlled_____

Sensitive Controlled_____

Requested Distribution:

To:

Copy:

EXECUTIVE SUMMARY

The Level 2 Milestone, L2.FMC.P11.01, "Demonstrate 3D PCI analysis with BISON-CASL for PCI fuel failure in a commercial power reactor", has been completed by the Fuels, Materials and Chemistry focus area of CASL. This report describes improvement in the BISON-CASL model for treating contact between fuel and cladding, documents the results of assessing fuel rod failure criteria against test reactor power ramp tests, and finally provides an assessment of the impact of power history and missing pellet surface (MPS) geometry on predicted maximum clad hoop stress and critical strain energy density based on the vendor provided power histories for both failed and non-failed fuel rods which operated in a U.S. commercial light water reactor that experienced fuel failures in the early 2000s.

The results of the BISON-CASL fuel performance modeling in 2D (R-Z or R-θ) are broadly consistent with current industry code capabilities, and the 3D modeling capability clearly provides a unique capability to industry. The fuel history from several fuel rods from a commercial reactor during operation in cycle 10 and startup to cycle 11 were used to evaluate the overall fidelity of the BISON-CASL fuel performance modeling. The BISON-CASL analysis demonstrated that both cladding hoop stress and SED increased significantly during the startup ramp between cycle 10 and the startup to cycle 11. The increase in these two possible failure indicators was caused by pellet-cladding mechanical interaction as a result of the fast startup ramp rate and the axial flux deviation. The BISON-CASL analysis in both 2D and 3D clearly indicated that the presence of a MPS was the cause for fuel rod M16S_O05 to have failed. Rods M19S_I02 and M12S_B06 both showed higher PCI stress values and thus it is possible that the failure of these rods was caused by either an MPS or possibly by some other mechanism, including a cladding corrosion assisted failure. Lastly, a demonstration of reactor startup power ramps has shown one possible power hold and ramp combination that has the ability to significantly reduce the maximum clad hoop stress and presumably minimize the potential for PCI related cladding failure. The potential for classical PCI based failures for higher burnup fuel than the rods analyzed in the current study remains for future consideration.

While this assessment demonstrates that BISON-CASL is evolving into a robust capability to provide mechanistic modeling and understanding for assessing PCI failure potential, several areas of further work and improvement were noted, including: 1) continuing to develop a robust 3-D contact algorithm utilizing less memory and better convergence success at high contact pressures; 2) a more robust smeared cracking model, which gives the ability to implicitly represent the fracture behavior of the ceramic UO_2 pellet to calculate crack formation, extension, and pellet mechanical compliance; 3) developing a relocation model that is informed based on the pellet-cladding gap; and 4) interfacing with a mechanistic model to assess stress corrosion cracking and crack propagation in the fuel clad. Further work on BISON-CASL will also focus on integrating micro-scale models under development in CASL-FMC that describe the irradiation creep and growth of zirconium alloys, the fracture, relocation, and mechanical compliance of the fuel pellet, and the release of fission products important for SCC (volatile and noble gases).

1. INTRODUCTION AND MILESTONE DESCRIPTION

Pellet cladding interaction (PCI) in light water reactor (LWR) fuel is a coupled thermal-chemical-mechanical process that can lead to cladding breach and release of radioactive fission products into the coolant under certain conditions of operating history, power change, and fuel rod design characteristics [1-4]. Reactor operating restrictions, which limit power maneuvering, have been established to mitigate PCI, but they restrain operational flexibility and lead to loss of power generation. The Consortium for the Advanced Simulation of Light water reactors (CASL) has selected PCI as a key challenge problem and is developing an advanced, 3-dimensional fuel rod simulation capability (referred to as BISON-CASL) to evaluate fuel performance in general and provide PCI failure assessments in particular. With an advanced fuel rod modeling capability that considers the underlying mechanisms leading to cladding failure, fuel designers and engineers can investigate improved fuel concepts for PCI-resistance and better quantify margins to PCI for operating existing fuel rod designs.

PCI failures generally occur following an increase in the local power over a short period of time, and in fuel that has been previously exposed to irradiation. Classical PCI is driven by the localized strains in the vicinity of a pellet crack, as well as the presence of a chemical species, such as iodine, that drive stress corrosion-induced cracking of the cladding [5,6]. Fuel pellet cracks that form in brittle ceramic pellets by large temperature gradients, are believed important in the PCI failure mechanism [5,6]. During a local power increase, pellet expansion produces a high contact force between the fuel pellet and cladding material, when a reduced or eliminated residual pellet-clad gap is present because of previous irradiation. Furthermore, during the rapid thermal expansion of the pellet, the fuel cracks can further open, which transfers tangential shear forces onto the cladding. These tangential shear forces are a function of the equilibrium pellet-clad gap or residual contact pressure at the start of the power increase, the power level at gap closure, the interfacial friction, and the maximum local power.

Non-classical PCI failure is associated with the presence of a missing pellet surface (MPS) defect [5,6]. These MPS defects form through mishandling or the manufacturing process, where the pellet is chipped leaving a flaw on the outer surface. The presence of an MPS defect during a localized power ramp can cause severe bending moments in the clad in the vicinity of the MPS when the fuel undergoes rapid thermal expansion due to this increase in local power. Furthermore, the localized region near the MPS also experiences a different temperature distribution compared to when the MPS is not present. The result is a localized hot spot in the fuel and cold spot in the clad.

Both classical and non-classical PCI are significantly influenced by the geometry of fuel pellet flaws (i.e pellet cracks and MPS). The purpose of this report is to assess the capability of BISON-CASL as a 3-D fuel performance code by modeling the fuel behavior in a US commercial power reactor, and comparing to actual hot-cell investigation data that indicated which fuel rods had failed. In the early 2000s, leaking fuel rods were observed in a US reactor following cycle startup, as well as a mid-cycle return to power [7]. The failed, or leaking rods, were all integral fuel burnable absorber (IFBA) rods, for which a root cause analysis concluded that the leakers were likely due to 'flaw assisted PCI, most likely a missing pellet surface (MPS)' [7].

Table 1 lists the commercial power reactor rods, which have been analyzed in this work, along with the rod average burnup and whether or not the rods failed [7,8]. It is important to acknowledge that detailed power history information has been provided by Exelon corporation [8], based on analysis performed by Westinghouse Electric Corporation. Table 1 also indicates that there are two rods from a single assembly (M16S_O05 and M16S_O04, respectively) which experienced similar rod average burnup and power history, but for which only one rod failed. This provides a strong opportunity for inter-comparison and assessment of the BISON-CASL fuel performance predictions for PCI/MPS failure. Figure 1 shows a cross-section of the rod M16-O05, which very clearly failed as a result of a missing pellet surface. The commercial power reactor fuel rods studied in this report provide a range of burnups from about 20 to 33 MWd/tU, and possible MPS geometries with which to assess the current state of BISON-CASL, and build upon past CASL reports and validation activities [5,6].

Table 1. List of commercial reactor fuel rods investigated in this CASL study [7,8].

Fuel rod identifier	Rod Average Burnup (MWd/tU)	Failed or non-failed
M16S_O05	20.7	Failed
M16S_O04	19.6	Non-Failed
M12S_B06	33.24	Failed
M19S_I02	31.6	Failed
M36S_D13	25.5	Non-Failed
M36S_M14	29.3	Non-Failed

The definition of this milestone explicitly states, "Demonstrate 3D PCI analysis with BISON-CASL on a relevant operating plant that experienced PCI failures." The remainder of this report will provide a brief introduction to the BISON-CASL fuel performance code (Section 2), document the activities within CASL to improve the modeling treatment of mechanical contact between the expanding fuel pellet and the fuel cladding (Section 3), and then describe the results of BISON-CASL assessments of fuel rod failure by comparing to ramp tests performed in test reactors (Section 4) before providing a comparison of BISON-CASL predictions to failed rods in a commercial power reactor (Section 5). Section 5 will also include a preliminary assessment of the impact of uncertainties in power history and MPS geometry on the predicted stress level in the clad. Section 6 concludes the report with a summary of the status and discussion for future efforts on fuel performance modeling.

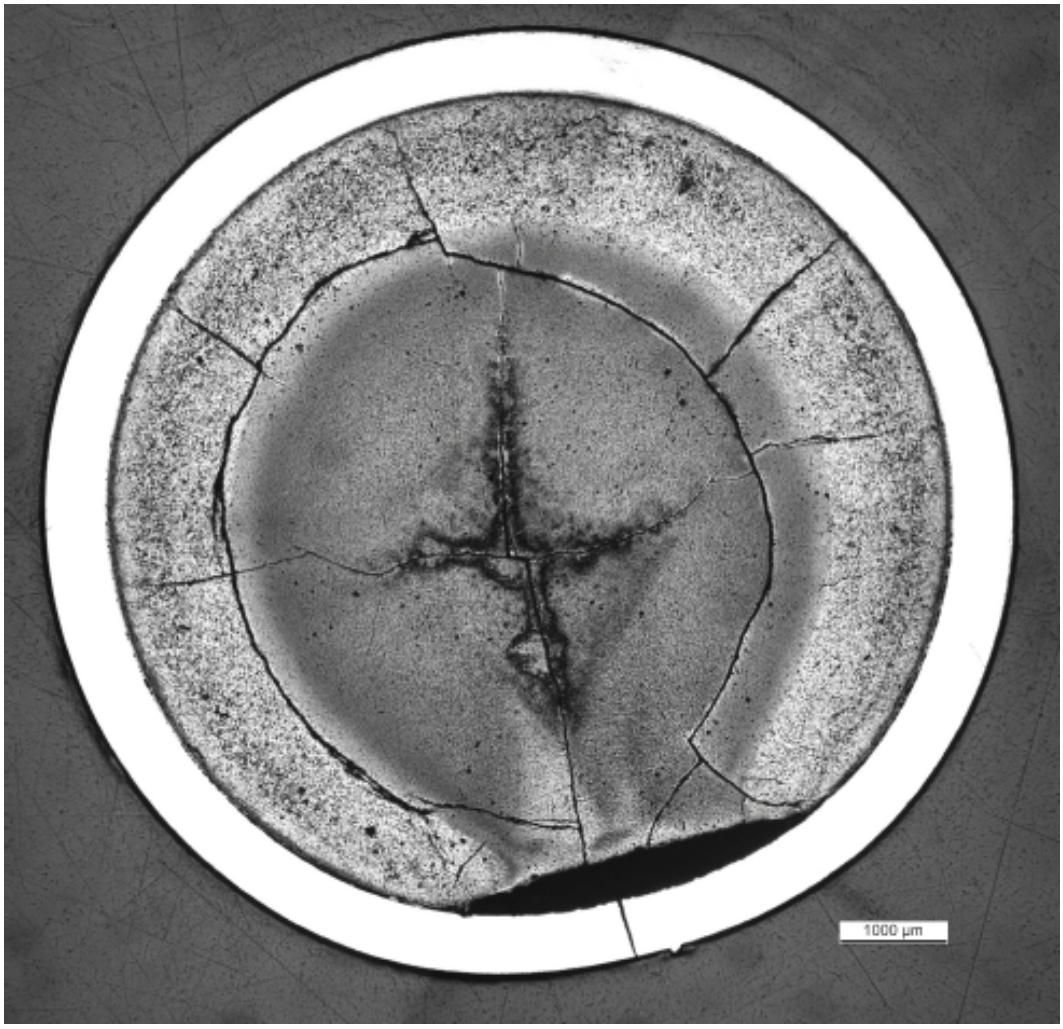

Figure 1. Cross-section of failed fuel rod M16_O05, as determined by hot-cell analysis, and reproduced from Ref. [7].

2. BISON-CASL MODELING OVERVIEW

The objective of developing an advanced, 3-D fuel performance modeling capability to assess PCI is to: 1) reliably calculate the cladding failure potential related to PCI; 2) define the impact of manufacturing flaws along with the material properties on failure probability; and 3) to evaluate the role of plant operating strategies as well as specific fuel designs on the PCI failure potential. To meet these objectives, it is imperative to develop a high-fidelity, fully coupled computer code that incorporates important plant operating procedures, e.g. power ramp rate and axial power shapes related to fuel performance, as well as considering the inherently coupled intricacies that occur in irradiated fuel behavior during normal and transient operations. By developing and employing a advanced fully coupled multi-physics and multi-dimension fuel performance code and developing mechanistic or physics based material models, efforts can be taken to reduce the uncertainties surrounding existing PCI failure methods. The approach to address the current uncertainties in PCI failure probabilities will allow for improved fuel utilization and increase the plant operating flexibility.

Again, the focus of the current report is to assess the capability of BISON-CASL as a 3-D fuel performance code to represent the underlining mechanisms controlling the failure of the cladding as a result of PCI, and in particular PCI driven by MPS, as compared to actual commercial nuclear power plant data. As mentioned in Section 1, the processes leading to cladding crack initiation and propagation begins with the presence of localized stress and strains in concert with available corrosive fission products. PCI fuel behavior modeling must be built upon a methodology that can reliably and consistently calculate the local stress conditions as a function of prior irradiation history, material properties, and local power conditions. This means capturing the effects of geometric irregularities (i.e. pellet cracks), permanent changes in dimensions of the pellet and cladding caused by fission product swelling and irradiation-induced cladding creep, as well as, thermal, mechanical, and chemical interactions between the pellet and cladding, i.e. frictional forces, heat transfer, and chemical bonding.

The assessment we perform within this work is summarized in Figure 2. The fuel rod analysis effort consists of four main steps that together are used to identify the effect of power operation on the PCI behavior of irradiated fuel. The first step consist of a steady state R-Z depletion analysis of the highest duty fuel, or the limiting rod, one with a known failure, is performed to establish the fuel rod conditions, e.g. pellet-cladding gap, plenum pressure, and released fission gas, following the first cycle of operation. The results of the steady state R-Z analysis provides the initial fuel rod conditions used in the third and fourth steps, which consist of analyzing the startup power ramp or a mid cycle power maneuver. The second step of the analysis consists of a full length R-Z analysis of the startup ramp. The purpose is to locate the region in the cladding were the maximum hoop stress is identified, using the R-Z power ramp analysis. Also the maximum hoop stress is generally located where the residual pellet-cladding gap is the smallest, e.g. gap at zero power.

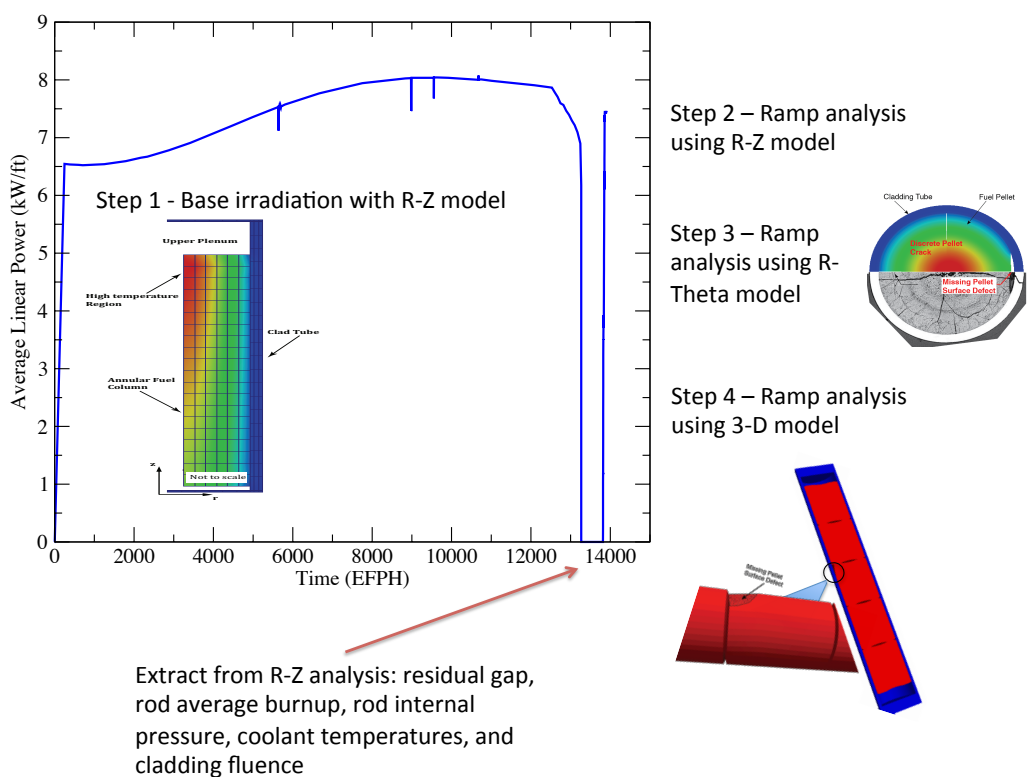

Figure 2. Workflow used in the assessment of PCI failures for a commercial nuclear power plant, as well as assessing failure criteria by comparing to test reactor power ramp data.

In the third step, the local cladding stresses and PCI damage index response are calculated using the R-θ local effects model at the peak stress location. This will be a specific PCI scenario and will be treated similar to the ramp test validation cases. However, these rod failures where contributed to PCI failure from a MPS. In the EPRI report [9] that analyzed PCI failures contributed to PCI, they assumed a single MPS size and did not consider the various sizes of MPS, as will be done here. Extending their analysis, we will investigate the impact of various MPS widths in addition to performing an evaluation of the impact of 3-D, length and width dependent MPS geometry. Similar to the third step, step four will evaluate the 3-D geometric effects on the local stress concentration, PCI damage index response, as well as critical strain energy density, and evaluate the failure potential for each rod in the assembly.

The purpose of the 3-D analysis will be to determine what the critical length and width of MPS will lead to a through wall failure. Along with studying the varying width and length effects of the MPS, an evaluation will be performed to assess the impact of ramp time on the three failure criteria. The purpose of this study will determine how the time it takes to reach full power affects the stress in the cladding along with how conditioning of the rod will assist in reducing the stress contributed to PCI.

2.1 BISON-CASL

BISON-CASL is built upon the Multi-physics Object-Oriented Simulation Environment (MOOSE) [10] developed at Idaho National Laboratory (INL). MOOSE is a massively parallel finite element computational system that uses a Jacobian-free, Newton-Krylov (JFNK) method to solve coupled systems of non-linear partial differential equations. In addition, the MOOSE framework provides the ability to effectively use massively parallel computational capabilities needed to create high fidelity 3-D models of a fuel rod, as well as full-length R-Z rods, and R-Theta geometric representation.

BISON-CASL builds upon the underlying architecture of BISON, developed at INL [11]. This architecture includes the ability to incorporate, or develop, material properties libraries and fuel behavior models for UO_2 fuel and zirconium alloy cladding commonly used in PWRs. A major focus of the CASL effort on modeling nuclear fuel performance, beyond the BISON-CASL development, has been to develop physics-based material models for ceramic UO_2 fuels and zirconium alloys [12]. These models consist of irradiation induced clad creep and growth, clad corrosion, the hydrogen pickup and hydride precipitation in the clad, and the release and transport of fission produced gas. However, since BISON-CASL is being developed simultaneously with the effort to develop improved mechanistic behavior models that are not yet ready for implementation, empirical models from the open literature and selected EPRI/Falcon models have been incorporated to date. This allows for testing of the numerical framework of BISON-CASL, as well as to identify material models that require further development.

3. IMPROVEMENTS IN MODELING MECHANICAL CONTACT

The Fuels, Materials and Chemistry (FMC) team within CASL, and in particular, the MOOSE/BISON team at Idaho National Laboratory has been focusing on developing improvements in the frictional contact enforcement capabilities in BISON. A robust capability for enforcement of mechanical and thermal contact

contact constraints is an essential aspect of a comprehensive nuclear fuel performance simulation code. Historically, contact has been problematic in BISON, but significant improvements have been made to the enforcement algorithms for mechanical contact (frictionless and glued) and thermal contact over the last couple of years. Until recently, the main focus has been on improving frictionless and glued contact enforcement, but now that those have become reasonably robust, efforts have shifted to improvement of frictional contact.

The biggest improvements to the robustness of enforcement of mechanical contact were made with the development of a new enforcement algorithm based on the Constraint system provided by MOOSE [13]. Because the Constraint system enables the correct entries associated with a constraint to be entered into the Jacobian matrix used for preconditioning, the mechanical contact enforcement algorithm based on that system offers drastically improved convergence of the linear iterations in the Jacobian-Free Newton Krylov solver used by MOOSE relative to the previous system.

Currently, the best preconditioning strategy for problems with mechanical contact in MOOSE is to use a direct solver. There are multiple options of packages to use for preconditioning, but in the BISON team's experience, the SuperLU package has been the most effective. One obstacle in the use of the Constraint system for contact has been that MOOSE was set up to allocate entries in the preconditioner for all possible contact interactions, which can result in large memory usage. Work performed earlier this year [14] addressed this issue by permitting a dynamic update of the set of nodes for which entries in the preconditioning matrix are computed. Since that time, a very difficult to find bug was corrected, which has resolved an issue in which the solver randomly crashed when this dynamic updating strategy was used.

With this work, BISON's ability to enforce frictionless and glued mechanical contact has become quite robust, and most existing models have been transitioned to the Constraint system, with good success. This has led to a vast improvement in the reliability of BISON in running the verification test suite. Until recently, the main focus of the efforts on mechanical contact has been on frictionless and glued enforcement. Frictional contact enforcement was originally developed in BISON prior to the development of the Constraint system, but it suffered from poor convergence rates. Frictional contact enforcement depends on a strong capability for frictionless and glued contact, so the focus was placed on improving those first.

Prior to the current work, there were two options for enforcement of frictional contact in MOOSE and BISON: a penalty algorithm and a kinematic algorithm based on a multilevel solution method.

Penalty Enforcement

The penalty algorithm is the simplest technique for enforcement of any kind of mechanical contact constraint, including frictional contact. At each contact node, the gap distance from the node to the contact point is computed. A penalty stiffness is multiplied by the gap distance, and a contact force is computed. For frictionless contact, only the normal component of the contact force is applied to the two interacting surfaces. For frictional contact, a tangential capacity is computed by multiplying the normal force by the friction coefficient. If the penalty tangential force exceeds that capacity, its direction is maintained, but its magnitude is limited to match the capacity in that direction.

For low values of penalty stiffness, the penalty contact algorithm is reasonably robust, but as the penalty stiffness increases, it becomes increasingly difficult to obtain a converged solution. Prior attempts to model quarter-length fuel rods with BISON with penalty contact were only successful with unacceptably low penalty factors that resulted in inaccurate solutions.

Multilevel Kinematic Enforcement

MOOSE also had a kinematic enforcement option based on the multilevel solution strategy described in [15]. In this strategy, there is an outer loop around the nonlinear solution. The contact constraints are treated as glued with strict kinematic enforcement in the inner solution loop, and after each inner loop is solved with the nodes glued, the solution is updated to permit nodes to slide if they exceed the frictional capacity. This is repeated until the sliding solution is converged.

While this approach is very stable, it also produces very slow convergence on long fuel rod problems on which it has been tested. Due to the nature of these problems, a very large number of slip iterations are required.

New Developments

Because neither the existing penalty or kinematic algorithms gave acceptable solutions on the problems of interest in BISON, improved approaches were sought. Work was conducted in the following major areas of as part of this recent work.

Penalty Enforcement

The previous work using penalty contact enforcement was all based on the legacy contact enforcement system in BISON rather than the Constraint system. When the constraint system was originally developed, a penalty frictional option was implemented alongside the other options, but this option had never been tested in 2D or 3D. This algorithm was tested for the first time, and improvements were made to the Jacobian matrix to account for the different behavior when nodes are sticking and slipping. Because the penalty enforcement is based on the new system with better pre-conditioning, solution robustness is significantly improved over the legacy system.

New Kinematic Enforcement

For frictionless and glued contact, the experience with BISON has been that the strict kinematic enforcement algorithm gives significantly better results than the penalty algorithm. Very high penalty factors have to be used to obtain solutions with acceptably small fuel/cladding penetration. For this reason, it is expected that a strict kinematic enforcement algorithm is also needed for frictional contact.

To overcome the slow convergence of the multilevel approach for kinematic contact on fuel problems, an entirely new method for kinematic enforcement of frictional contact has been developed. The residual is computed in the constraint enforcement code in a manner that permits the nodes to slip if they have exceeded the frictional capacity, while enforcing the Kuhn-Tucker conditions governing the slip behavior. This approach has been implemented and successfully verified on test problems.

Contact Slip Damper

Obtaining a converged frictional contact solution is challenging regardless of the interface behavior because of the discontinuities that occur as nodes move in and out of contact. Frictional contact introduces additional challenges because of the discontinuities arising from the stick-slip conditions that are enforced. There are discontinuities in the contact force as a node moves between sticking and slipping states, and the contact force changes directions as the direction of slip changes. These discontinuities make solution of the nonlinear system of equations extremely challenging.

To manage this highly discontinuous behavior and obtain converged solutions, an algorithm has been developed to monitor the nonlinear iterative solutions to check for changes in the slip direction from one iteration to the next. If a change in the slip direction is detected, the iterative update to the solution is scaled back to prevent nodes from oscillating between solutions that slip in opposite directions. This problem can be particularly severe with the kinematic enforcement algorithm, and this damping approach has been successfully applied to improve the convergence of problems with both kinematic and penalty enforcement.

Testing

In addition to the algorithmic improvements described above, a large component of the recent work on frictional contact has been on testing. This testing has consisted both on developing a set of verification problems to compare with known solutions and on testing with a fuel problem. There are a number of contact problems with known solutions available in the literature. Developing a set of finite element models of these problems is an essential step in the development of a contact enforcement capability to test the robustness of algorithms and ensure that they give accurate solutions as they are developed. To that end, an initial set of 2D and 3D contact problems has been developed to verify the implementation of frictional contact in BISON, as was reported earlier this year in milestone report L3:FMC.PCI.P11.02.

A subset of those problems is presented here with the solutions obtained for those problems to demonstrate BISON's current capabilities for frictional contact.

Sliding Sphere (3D)

Hertzian contact between a sphere and a rigid surface is a classic problem within contact mechanics. A 3D model was setup in BISON and the geometry and mesh is shown in Figure 3. The rigid block is fixed in all directions and normal and tangential displacement boundary conditions are applied to the surface nodes of the half sphere.

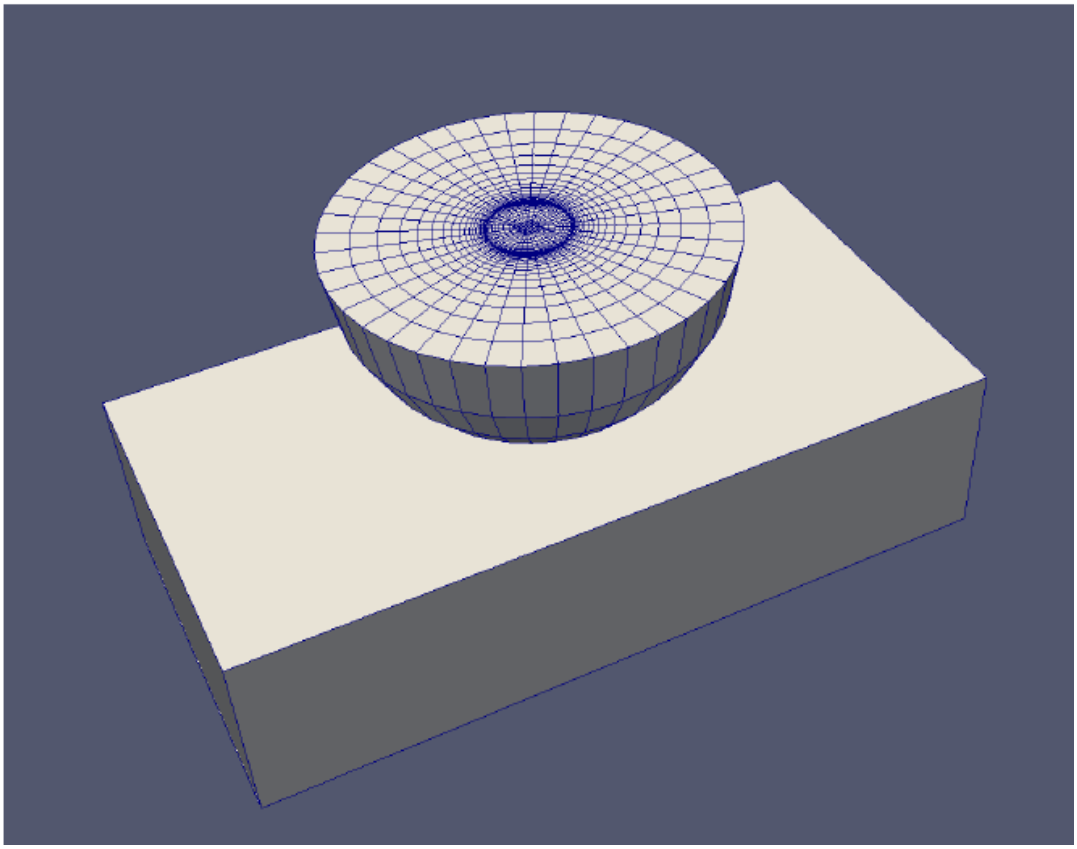

Figure 3. Geometry and mesh of 3D sphere sliding on a block, used as a 3D test problem for assessing the robustness of the modeling treatment of mechanical contact.

The normal stresses on the surface of the sphere in contact after the sliding phase of the analysis are shown in Figure 4. The sphere was slid to the right in the analysis and the normal stress contours shift to the left in a similar fashion as observed in the 2D cylinder example. This model was run using the penalty contact option. Work is in progress to run this using the kinematic enforcement algorithm.

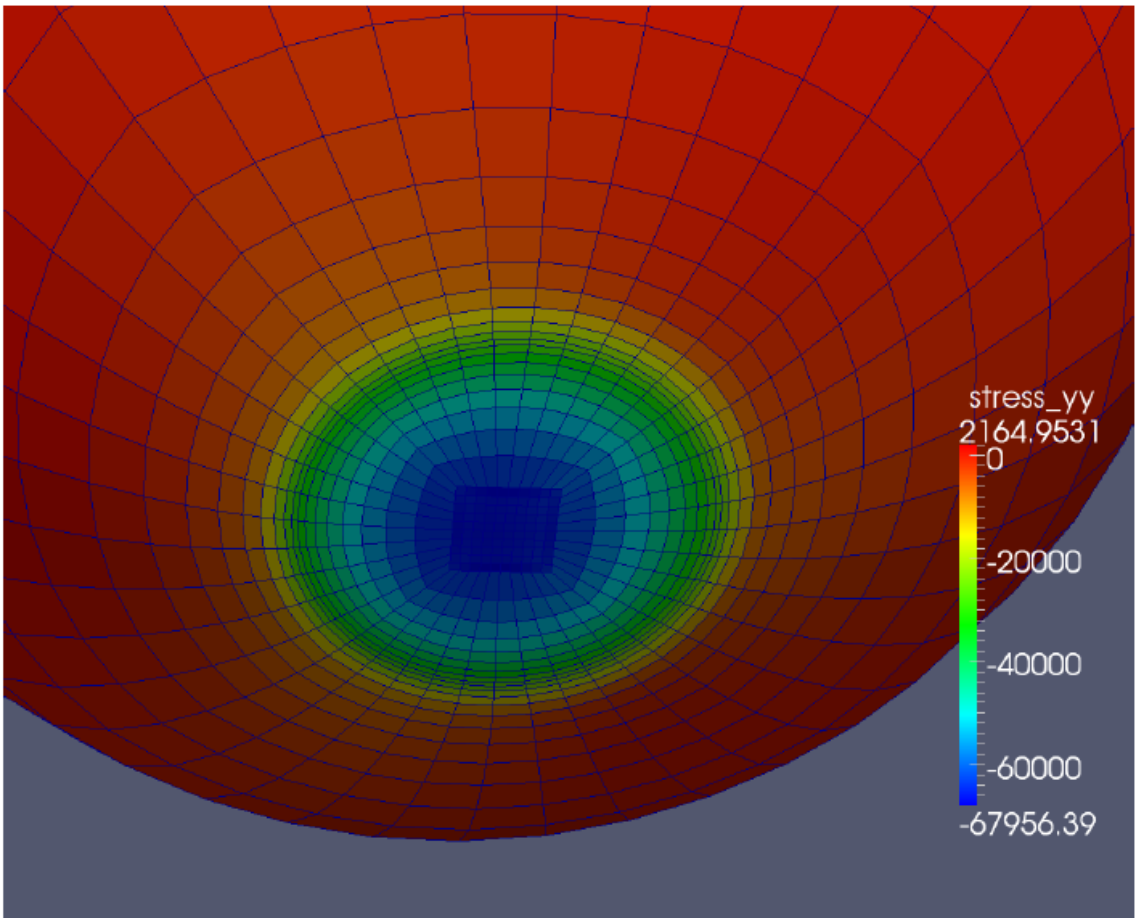

Figure 4. Normal stress on 3D sphere sliding on a block.

2D Fuel Rod Demonstration

The new kinematic frictional contact algorithm has been tested on the IFA 431, Rod 3 experiment tested in the Halden reactor. This is a test of a quarter-length rod with thermocouples at the top and bottom. The series of rods tested had a variety of gap sizes, with some of the experiments having significantly smaller than standard gaps. The experiments had live monitoring of the fuel rod elongation, which makes them useful for benchmarking frictional contact models.

An earlier attempt to model this rod in BISON experienced significant convergence challenges. One of these test cases was run with the new kinematic contact algorithm, and successfully ran to completion. That model had an artificially small gap in an attempt to capture the effects of pellet eccentricities on fuel rod elongation. This particular model experiences contact very early on in life, first at the top of the fuel column, and a significant number of the nodes enter sticking contact.

BISON was able to obtain a converged solution with relatively little difficulty on this model using the new kinematic enforcement algorithm with the frictional contact damper. Figure 5 shows a representative result with the tangential traction magnitude contour for this model. The study of this problem is by no means complete, but the recent improvements are expected to enable a suite of models of this experiment to be run. Future efforts will continue to evaluate modeling improvements for the treatment of mechanical contact to improve the fidelity of both 2D and 3D fuel performance simulations using MOOSE/BISON.

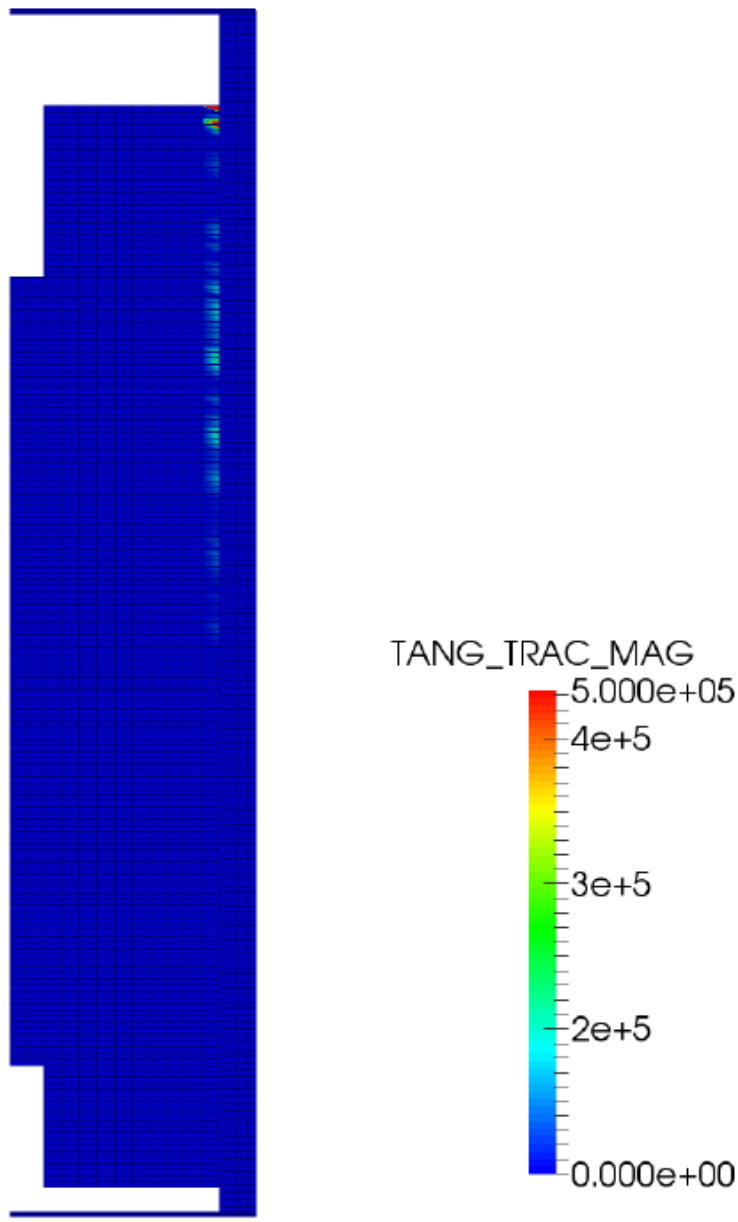

Figure 5. Magnitude of the tangential traction calculated in BISON for a 2D, R-Z fuel performance simulation of IFA 431 Rod 3 fuel test. The axial dimension has been scaled by 0.05.

4. BISON-CASL MODELING OF RAMP FAILURE TESTS

4.1 Approach

The objective of the current effort has been to develop a fuel performance modeling methodology to calculate, using commercial data, when and where a fuel rod failure will occur. However, before this goal can be achieved, we must first develop some confidence in an appropriate metric for failure analysis based on comparisons to ramp test data performed in test reactors. The test rods chosen for this assessment were obtained from a number of experimental ramp test programs that utilized irradiated commercial PWR rods to conduct rod failure experiments following a significant power maneuver. These included the Studsvik Over Ramp, Super Ramp, and Trans Ramp IV programs [16-18], as well as, rods from a CEA/OSIRIS ramp test

program [19]. The data for these tests were extracted from the IFPE, the OECD/NEA International Fuel Performance Experiments database [16-19]. Detailed information on these test programs is available in the project reports that are also contained in the IFPE [16-19]. The goal of this work is to demonstrate the methodology for 3-D PCI analysis, as discussed above, and determine the differentiation between failed and non-failed rods, the test inventory included rods that failed during ramp testing as well as those that survived. A list of all the experimental ramp test rods used in the current assessment is shown in Table 2.

TABLE 2. PCI Ramp Test Rod Database for Failed and Non-Failed Fuel Rods [16-19].

Ramp Test Experiment	Burnup (MWd/tU)	Failed Rods	Non-Failed Rods	P_{cond}(kW/m)	P_{max}(kW/m)
RISO FGP3	42-43	0	2	25-29	39-40
SuperRamp	35-45	5	10	25	35-49
TransRamp II	31	3	3	20	42-60
TransRamp IV	23-29	5	2	25	43-45
OverRamp	16-23	7	8	30	37-45
Osiris	23-25	0	2	21-24	39-43

P_{con} – Ramp Conditioning Power
P_{max} – Ramp Terminal Power

The ramp tests conducted for each of these cases followed a similar approach. After base irradiation in a commercial PWR, the rods were examined to measure cladding diametral deformation and then refabricated for use in the ramp tests. The ramp tests were conducted in test reactors by first conditioning the rods at a moderate power level (20 to 30 kW/m) for hold periods of typically 24 hours. A power ramp was then initiated at a prescribed ramp rate to a final P_{max}. The power was then held at the peak ramp power level for a period of time or until rod failure was detected, depending upon the goal of the particular test. Post-ramp PIE of the rods typically included rod length, profilometry, and fission gas release measurements, as well as visual inspections and neutron radiography. Destructive examinations were also often conducted to provide detailed information on the nature and location of the fuel rod failures experienced in the tests. However, the majority of the ramp test do not contribute rod failure to MPS but do contribute it to classical PCI. Data from these examinations are available in the IFPE [16-19]. Figure 6 illustrates the typical ramp test power history used in the majority of these tests.

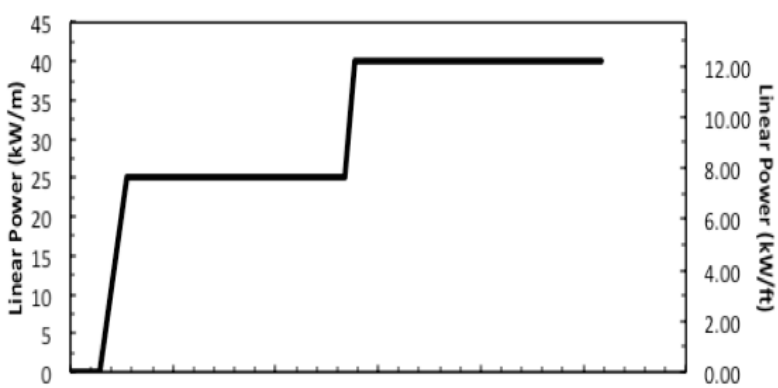

Figure 6. Typical ramp test power history, beginning with a conditioning power (P_{con}) and ending with a ramp to terminal power (P_{max}).

4.2 Results

Each of the experiments listed in Table 2 contain a number of rods for analysis. However, due to time constraints, only a few select fuel rods have been analyzed to date. The rods that were chosen came from the OverRamp experiment [17]. The results of these simulations were compiled and compared to previously reported results available in the literature [20], where applicable. For example, comparisons were made to available cladding creep down post-irradiated examination (PIE) data.

Comparisons to available PIE data provided a metric to establish the accuracy of the BISON-CASL calculations for the base irradiation. Key to performing the PCI analyses is the proper determination of the fuel-cladding gap prior to the ramp test. The accuracy of this parameter is an indicator of the accuracy of the base irradiation modeling and is required to properly set the initial conditions used during the subsequent modeling of the power ramp to accurately reflect the conditions in the experiment. The two parameters that determine fuel-cladding gap are fuel radial expansion and cladding creep down. Unfortunately, there are no measured values for fuel-cladding gap or fuel radial expansion, but there are experimental determinations of cladding creep down available.

Table 3 shows four different methods used to apply plenum and coolant pressure to the surface of the cladding. The table then compares the resultant cladding creep down values to the experimentally measure values. This sensitivity study shows the current capabilities in BISON-CASL. It was important to understand how applying the pressure boundary conditions would affect the resultant cladding creep down. Currently, BISON-CASL does not have the capability to model a plenum spring. The purpose of the plenum spring is to minimize the mobility of the fuel, but also exerts an axial force on the cladding as well. This axial force opposes the pressure seen from the coolant, more or less canceling it out. For this reason method 2 seemed the most appropriate pressure boundary condition. Method 2 assumes the plenum pressure and plenum spring cancel out the coolant pressure on the top and bottom of the cladding. This assumption results in the plenum pressure being applied to the inner tube surface of the cladding, and the coolant pressure being applied to the outer tube surface of the cladding.

Table 3. Pressure boundary condition sensitivity study, comparing different plenum and coolant pressure boundary conditions to the experimentally measured cladding creep down values.

	W4-1	W4-2	W5-4	W5-5	W5-6
Experiment	16.5	18	21.5	28.5	28
Method 1	13.19	13.45	17.01	19.62	27.05
Method 2	20.43	21.78	23.3	26.69	27.56
Method 3	17.74	23.02	24	27.91	28.26
Method 4	12.14	16.42	18.33	21.2	21.2

Method 1 – Applied coolant pressure to top, outer surface, and bottom of clad. Applied plenum pressure to inner surface of the clad.

Method 2– Applied coolant pressure to outer surface of clad. Applied plenum pressure to inner surface of clad. No pressures where applied to the top and bottom of the clad.

Method 3 - Applied coolant pressure to outer surface of clad. Applied plenum pressure to top, inner, and bottom surface of the clad.

Method 4 - Applied coolant pressure to top, outer surface, and bottom of clad. Applied plenum pressure to top, inner, and bottom surface of the clad.

Other sensitivity studies were conducted, such as relocation activation energies, relocation stop parameter, fuel creep, and fuel densification parameter. The relocation activation energy determines the linear power for fuel relocation to occur, and relocation stop determines the rod

average burnup at which fuel relocation is no longer allowed to occur. BISON-CASL is currently implementing a smeared cracking model, which allows the fuel to crack and expand when stresses are high enough. Without a smeared cracking model, stresses in the fuel will increase until fuel creep occurs. As the fuel creep occurs it softens the compliance of the fuel as well as reduces the fuel's radial expansion. By reducing the fuels ability to radially expand, this causes the residual gap to be much larger than expected. Based on those results, it was determined that fuel creep should not be included in the modeling. However with fuel creep turned off, BISON-CASL then over-predicts the fuel radial expansion. This contributed to the fuel densification parameter being too low. The fuel used during the OverRamp experiment was an older fuel design and was considerably less stable than modern fuels. The stability is a contributing factor to how much irradiation-induced densification can occur. With the OverRamp fuel being older fuel, it was determined that 1% fuel densification is a reasonable amount of irradiation-induced densification. Below is a brief summary of the boundary conditions, models, and parameters used, and Table 4 summarizes the final results following the base irradiation.

R-Z Problem Set Up

- Coolant and Plenum Pressures
  - Pressures are only applied to cladding inner and outer tube surfaces
- ESCORE Relocation Model
  - Activation = 5 kW/ft
  - Stop = Rod average burnup at the end of the base irradiation
- Fuel Creep
  - Turned off, BISON-CASL does not currently have reliable smeared crack model
- Fuel Densification
  - 1%, Ramp test used older fuel which is unstable allowing for more densification to occur

Table 4. Dimensional Changes Following the R-Z Base Irradiation.

	W4-1 (F)	W4-2 (NF)	W5-4 (NF)	W5-5 (NF)	W5-6 (F)
Rod Avg Burnup (MWd/tU)	19.02	19.07	15.25	20.7	20.7
Exp Clad Creep Down (microns)	16.5	18	21.5	28.5	28
Sim Clad Creep Down (microns)	20.43	21.78	23.3	26.69	27.56
Fuel Radial Disp (microns)	33.45	33.42	23.11	35.64	35.44
Gap Thickness (microns)	28.62	27.78	36.09	19.88	19.5
Fast Fluence*e25 (n/m^2)	1.85	1.97	1.67	2.07	2.11
Plenum Pressure (MPa)	3.17	3.25	1.73	1.78	1.61

F – Rod that failed

NF – Rod that did not fail

Before a PCI ramp analysis can be done to assess the appropriate fuel rod failure criteria, a sensitivity study of the mechanical contact between the fuel and clad needed to be conducted. This study looked at how changing the coefficient of friction (CoF) between the fuel and clad would affect hoop stress on the inner surface of the cladding. Once the gap closes and a power transient occurs the fuel's radial cracks begin to open and slide across the claddings inner surface. The fuel resistance to sliding causes a concentration of tangential stresses to build on the claddings inner surface. The CoF allows for the fuel to gain more traction on the claddings surface, which results in an increase in the hoop stress. Figure 7 shows the relationship between cladding hoop stress and CoF. As seen in Fig. 7, an increase in the CoF produces a corresponding significant increase in the peak hoop stress. Furthermore, the expectation is as the CoF extends past a value of 1 to infinity (shown on the plot as CoF=2), the peak hoop stress will begin to converge toward the value obtained when modeling the contact as glued, which is shown as a red circle in Figure 7.

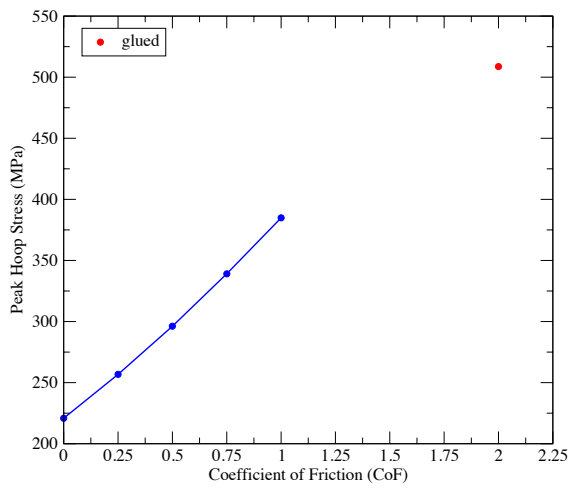

Figure 7. The relationship between peak hoop stress (y-axis) and the coefficient of friction (CoF) (x-axis) for 2-D R-Theta models, in which glued contact is considered to be CoF = infinity.

Choosing a CoF to use for the PCI analysis is a difficult task. At lower burnups, the outer fuel surface is considered to be smoother as is the inner clad surface, which has had less time for internal corrosion. Both of these will allow more slippage in the fuel, resulting in a lower CoF. However, higher burnup fuel has a rougher surface and the cladding will have fission product corrosion creating a stickier surface, resulting in a higher CoF. The OverRamp rods are lower in burnup, therefore a CoF of 0.75 was chosen for the 2-D R-Theta modeling assessment. Contact in 3-D is significantly more complicated. To simplify contact for the 3-D simulations, we have assumed glued contact in the 3D BISON-CASL ramp test modeling. The peak cladding hoop stress and strain energy density (SED) results from the OverRamp rod analyses are summarized in Table 5 for the non-failed and failed rods, respectively.

Table 5. Peak hoop stress and strain energy density (SED) values calculated using BISON-CASL in 2D (R-Z, R-Theta) and 3-D.

	W4-1 (F)	W4-2 (NF)	W5-4 (NF)	W5-5 (NF)	W5-6 (F)
Burnup (MWd/tU)	19.02	19.02	15.25	20.7	20.7
2-D R-Z (MPa)	93	75.2	30.3	112	140
2D R-Theta (MPa)	437	330	301	525	529
2D R-Theta (SED in MJ)	1.45	.862	.74	2.03	2.09
3D R-Theta (MPa)	348	160	146	371	420
3D R-Theta (SED in MJ)	1	.359	.197	1.15	1.25
Falcon 2-D R-Theta (MPa)	N/A	N/A	291.8	453.2	474.2

F – Rod that failed

NF – Rod that did not fail

Based on the results summarized in Table 5, a comparison of rods with similar burnup (e.g. W4-1 compared to W4-2 and W5-5 compared to W5-6), indicates that the failed rods have higher calculated stresses and strain energy density (SED) than do non-failed rods. This is true for both the 2D (R-Z and R-Theta) and 3-D simulations performed with BISON-CASL. When comparing calculated hoop stresses in the R-Z simulations to the PCI simulations, the hoop stress is expected to be significantly higher in the PCI simulations. This is because the existence of radial cracks causes significant stress concentration in the fuel clad [5,6]. During the transient increase in power, radial cracks open and the coupled opening of the cracks plus the closure of the pellet-clad gap produces an increase in both the hoop stresses and the SED in the cladding. For classical PCI simulations, there should be no significant difference between the stress levels calculated by a 3-D versus a 2-D model, however there may be some potential differences between the calculated SED. This stems from the 3-D model accounting for axial expansion, and SED is calculated using the tri-axial stress state. The fuel tends to expand more axial than the cladding, and this difference in axial expansion can cause increased axial stresses in the cladding. When comparing the 2-D stress and SED values to the 3-D stress values it is very clear there is a significant difference. Figure 8 shows a comparison of fuel clad gap and fuel centerline temperature, as a function of time using 2D or 3D modeling with either no initial burnup, or a value of 0.019 fraction of initial heavy metal atoms (FIMA), which can help explain why there is such a significant difference between the calculated hoop stress values in the clad.

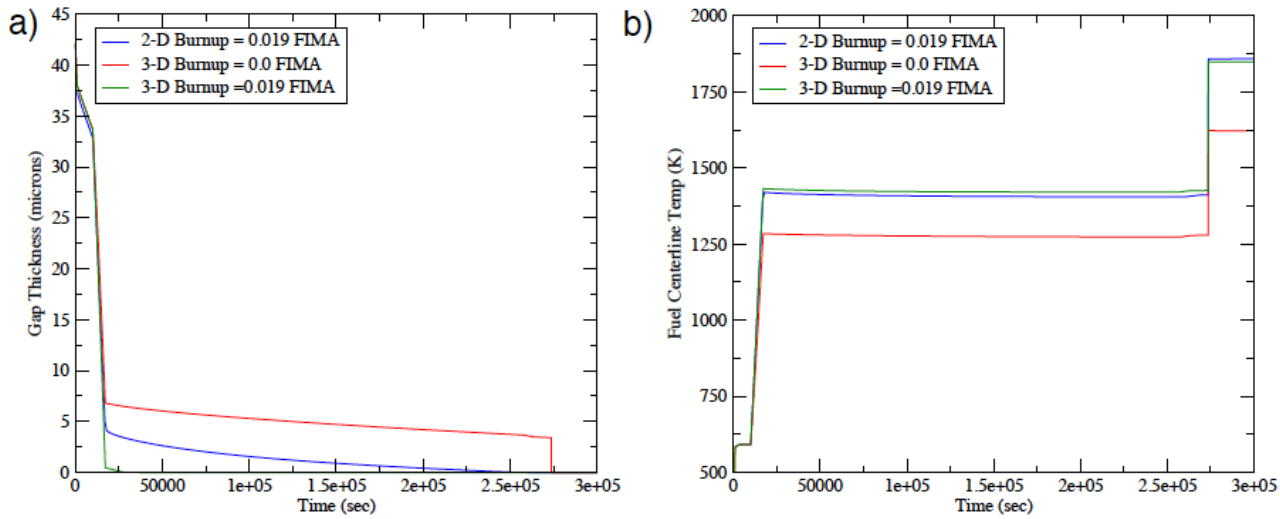

Figure 8. (a) W5-4 gap thickness comparison between a 2-D simulation with an initial burnup = 0.019 FIMA (blue), to a 3-D simulation with an initial burnup = 0.0 FIMA (red), and 3-D simulation with an initial burnup = 0.019 FIMA and (b) Fuel centerline temperature for the same three simulation cases.

Looking at the gap thickness comparison, Fig. 8a, there is a clear difference between the three simulations. The two potential differences are either the fuels radial expansion or the claddings creep down. The irradiation time for this simulation is ~3 days, and thus, the leading candidate for the discrepancy would be the fuel. Fig. 8b indicates that there is a clear, ~130 K, difference between the fuel centerline temperatures. Upon further investigation it was determined the 2-D models accounts for the accumulated burnup during the base irradiation and the original 3-D model (red) does not. The burnup accumulation during the base irradiation causes a significant reduction in the fuel thermal conductivity. With the 3-D simulation (red) being treated as fresh fuel, its thermal conductivity will be significantly higher than used in the 2D simulation, which would result in temperature differences leading to differences between the fuel radial expansion. For the OverRamp simulations with similar burnup, it is to be expected that burnup could be treated as a scaling variable, which would increase the 3-D stresses and SED to comparable values seen in the 2-D results. However, comparing the 2-D and 3-D results separately should give us a good indication of our failure analysis assessment. For a true failure analysis the 3-D simulations would need to account for the accumulated burnup, show in Figure 8 with a green line. However, 3-D contact is not robust enough to account for the higher contact pressures, and fresh fuel is assumed for the remainder of the 3-D simulations.

To develop a failure threshold limit, whether stress, SED, or CDI, every rod needs to be compared equally and not separately. Figure 9 and 10 summarizes the failed and non-failed rods stresses and SED as a function of burnup. Fig. 9a and 9b shows the data are scattered and that there is not a true failure threshold stress or SED. SED appears to have a little more separation between failed and non-failed rods, but as previous studies have shown, the more data that populates the graph, the more this distinction in failure threshold is blurred [5,6]. The 3-D stress and SED values seem to give a little more separation between both stress and SED values, but there is still not enough data to determine a failure value. Again as the graph is populated with more data it is anticipated to blur the lines between failed rods and non-failed rods, similar to the 2-D analysis.

Correspondingly, in the remainder of this report, both maximum hoop stress in the clad and the strain energy density will be calculated and compared to the commercial power reactor fuel rod performance data of whether rods failed or not. However, it is clear that the current state of failure

probability assessment is unsatisfactory, and work will continue in the future to provide a more mechanistic approach to assessing failure.

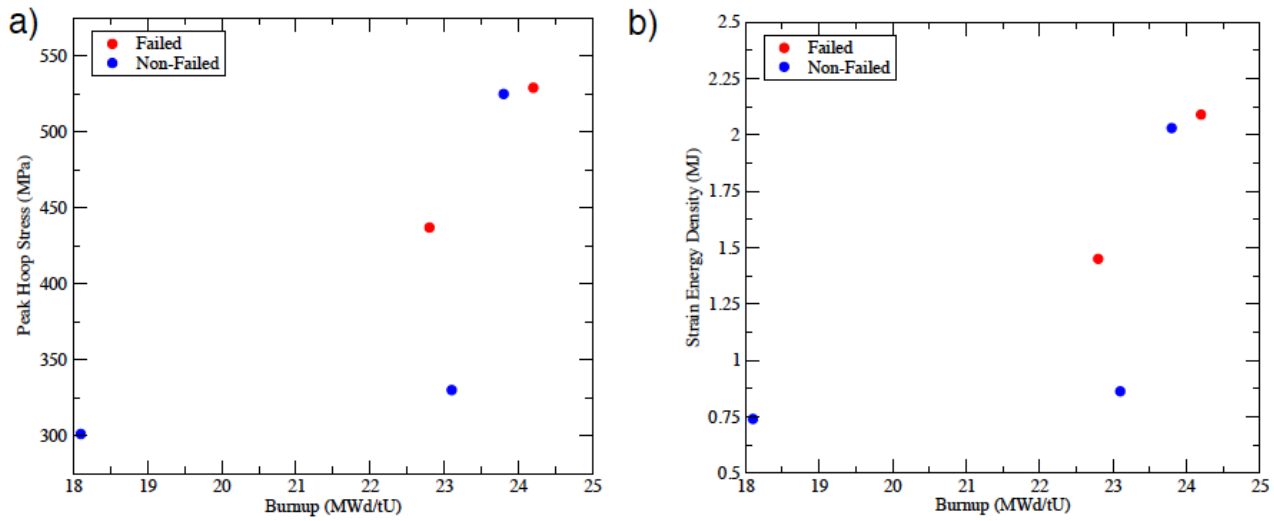

Figure 9. 2-D modeling results of ramp tests assessing the appropriateness of a failure probability based on a) peak hoop stress or b) strain energy density, as a function of burnup.

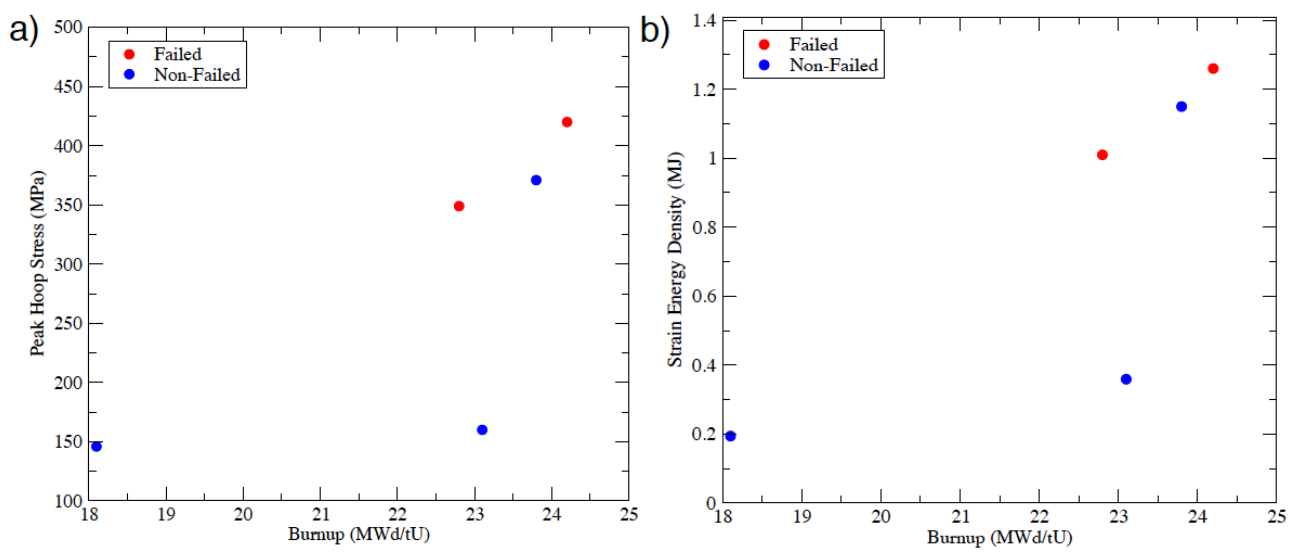

Figure 10. 3-D modeling results of ramp tests assessing the appropriateness of a failure probability based on a) peak hoop stress or b) strain energy density, as a function of burnup.

5. BISON-CASL MODELING ASSESSMENT OF FAILED AND NON-FAILED FUEL RODS IN A COMMERCIAL POWER REACTOR

5.1 Approach

Westinghouse provided data required to construct a full-length model (R-Z geometry) used to analyze the selected commercial reactor fuel rods with BISON-CASL using the steady state, startup power histories, and axial power profile [8,9,21-24]. The full-length R-Z model analyses will be used to identify the axial location with the highest cladding hoop stress, and also to determine the fuel-cladding gap condition, following the

stead state cycle, for the more detailed local PCI analysis with the R-θ slice model and a more detailed 3-D 5 pellet model. The principal fuel rod design parameters used in the analysis are shown in Table 6.

Models for a Westinghouse 17x17 IFBA fuel rod were constructed with detailed fuel design data supplied by Westinghouse. In addition to the geometric mechanical model, a detailed power history which captures sufficient spatial and temporal power resolution to model both global and local conditions must be developed for a reliable PCI analysis. Exelon and Westinghouse have provided a detailed steady-state and power ramp data which has been used to construct the necessary power histories for the BISON-CASL analyses, which is shown in Figure 11. The rod average power history, Fig. 11a, maintains a relatively constant linear power of 4 kW/ft and increases linearly to a final power of 5.25 kW/ft followed by a power down at the end of cycle 10. However, the power at the location of peak power begins by a rapid increase to 5.5 kW/ft, then remaining relatively constant with a few instances of increasing in power until reaching 6-6.5 kW/ft. Following the end of cycle 10 is the startup of cycle 11, as detailed in Fig. 11b. Rod failure was observed for this commercial reactor during the cycle 11 startup, for which the peak power location reaches a significantly higher power than the rod average. The peak power position causes the pellet-cladding gap to close faster, leading to a smaller gap upon the startup of cycle 11. This is the axial location where a PCI related failure would most like occur.

The fuel rods described in Table 6 use a ZIRLO™ cladding. CASL does not have material property data and models for ZIRLO. However, data previously supplied by Westinghouse and analyzed in the literature [21,25] indicates that the creep and irradiation growth of ZIRLO can be effectively modeled by reducing the corresponding models of Zircaloy-4 by 20% [26-28], as has been done in this analysis.

The failed fuel rods from the commercial reactor contained a unique burnable absorber, ZrB_2, which is placed as a thin coating on the fuel pellet outer circumferential surface, and referred to as an integral fuel burnable absorber, IFBA pellets [9]. The neutron capture by B-10 produces He and Li atoms, which are initially entrapped in the ZrB_2 layer. The helium will ultimately escape to the fuel rod void volume, thus changing the fill gas quantity and rod internal pressure. A special model for the helium release from the ZrB_2 coated pellets will need to be developed for BISON-CASL based on information of the release rate, provided by Westinghouse. The information for this model was not received in time, so for the purposes of this report BISON-CASL assumed there was not an IFBA layer. This will result in lower plenum pressure and more cladding creep down.

Table 6. Westinghouse 17OFA fuel rod parameters needed for commercial PWR analysis, as obtained from Ref [4].

Rod Description	Value
Cladding outer diameter (inch)	0.360
Cladding inner diameter (inch)	0.3375
Cladding Material	ZIRLO™
Cladding surface roughness (micro-inch)	16
Pellet outer diameter (inch)	0.3088
Pellet surface roughness (micro-inch)	80
Radial gap (mils)	28.7
Enrichment (%)	4.6-4.95
Fuel density [% of T.D.]	95
Internal gas pressure [He] (psig)	275
Dished pellet	Yes
Fuel stack length (inch)	144.0

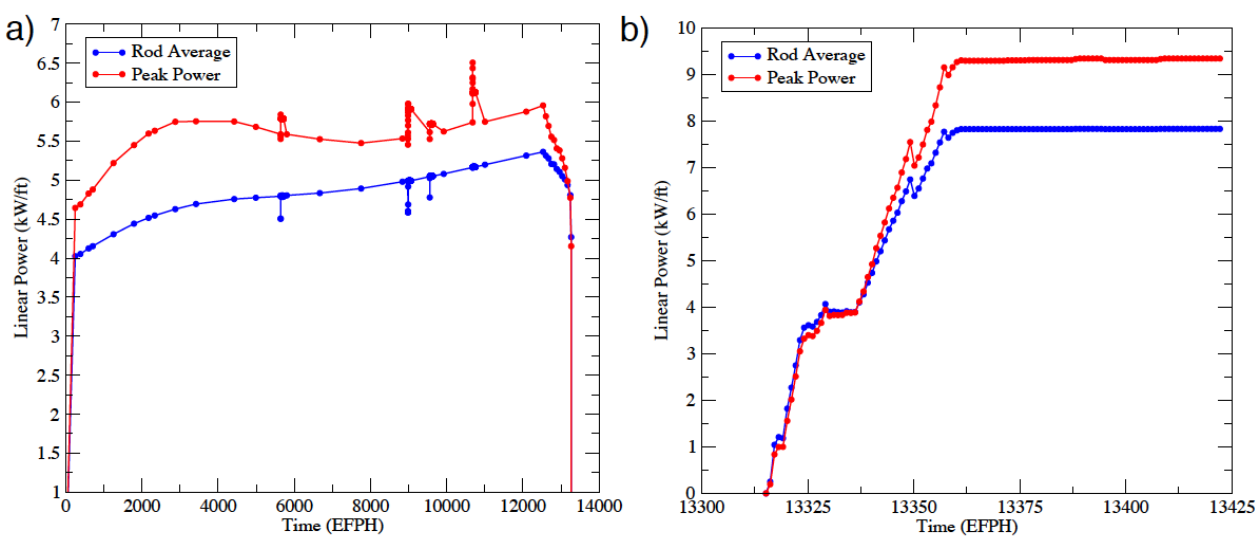

Figure 11. Average power history (blue) and the linear power at the axial location corresponding to peak power (red) for fuel rod M16S O05 a) during cycle 10 operation at a commercial power plant and b) during the cycle 11 startup, as obtained from [9].

5.2 Results

In order to identify the maximum cladding hoop stress location during the startup of cycle 11 in a commercial power reactor, a full-length BISON-CASL R-Z analysis was performed for the selected fuel rods using the cycle 10 and cycle 11 power histories, which were obtained from Exelon and Westinghouse [7]. With this approach, the magnitude and axial location of peak cladding stress were identified during cycle 11 startup. The R-Z analysis results from cycle 10 were then used as initial conditions to model the local effects of PCI in 3D during the cycle 11 startup.

Based on the failure assessment sensitivity work described in section 4.2, the same methodology was used to evaluate both the cycle 10 and cycle 11 startup. The conditions for the R-Z simulations are listed below, with the only change being the densification parameter. This change from the previous ramp test analysis was made based on the fact that the Westinghouse fuel used in the commercial reactor was more stable than early fuel forms used during ramp test program, and this would result in less densification occurring.

R-Z Problem Set Up

- Coolant and Plenum Pressures
  - Pressures are only applied to cladding inner and outer tube surfaces
- ESCORE Relocation Model
  - Activation = 5 kW/ft
  - Stop = Rod average burnup at the end of the base irradiation
- Fuel Creep
  - Turned off, BISON-CASL does not currently have reliable smeared crack model
- Fuel Densification
  - .05%, Ramp test used older fuel which is unstable allowing for more densification to occur

Many of the cycle 10 rods experienced higher nodal power during the cycle 10 base irradiation when compared to non-failed rods from cycle 9. The specific power history for cycle 10 and the startup of cycle 11 are shown in Figure 12, for both failed (a and b) and non-failed (c and d) rods. Assembly M36S contains the most aggressively operated rods, for which the fuel rod M36S_D13 reached a peak nodal power of 10 kW/ft during cycle 10. Correspondingly, these rods accumulated higher rod average and nodal burnup. However, several rods, including those designated as M19S_I02, M12S_B06, and M36S_M14 experienced comparatively smaller power changes during the cycle 11 startup than the failed rod, which was M16S_O05.

Fuel rod M16S_O05 has a much lower rod average burnup compared to the other non-failed rods, but it experienced the largest change in power between the cycle 10 coast down power and the cycle 11 startup. As the M19S_I02, M12S_B06 and M36S_M14 rods have experienced higher nodal power during the Cycle 10 base irradiation, the pellet-cladding gaps for these rods closes after about 350 EFPDs, within their first cycle, in the reactor. Comparisons between BISON-CASL and Falcon fuel performance assessments of fuel – clad gap and displacements for rod M12S_B06 are shown in Figure 12, and again provide confidence that BISON-CASL is predicting similar quantitative results to Falcon.

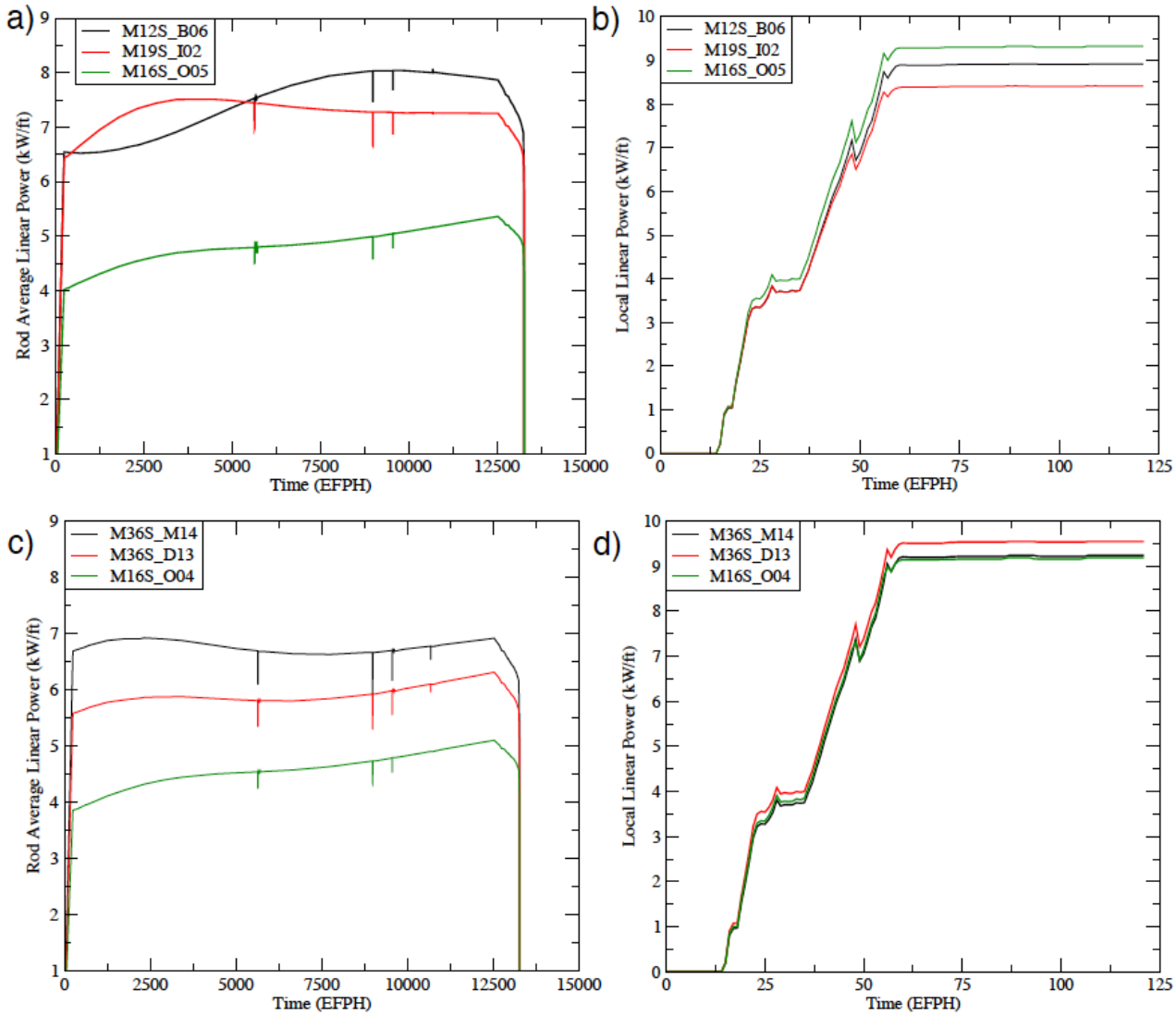

Figure 12. Power histories for failed and non-failed fuel rods within a commercial nuclear power plant during cycle 10 and the startup of cycle 11. a) cycle 10 power history for three rods which subsequently failed, b) local linear power at the axial location of peak stress during cycle 11 startup. c) cycle 10 power history for three rods which did not fail, and d) local linear power at the axial location of peak stress for the three non-failed rods during cycle 11 startup of a commercial nuclear power plant.

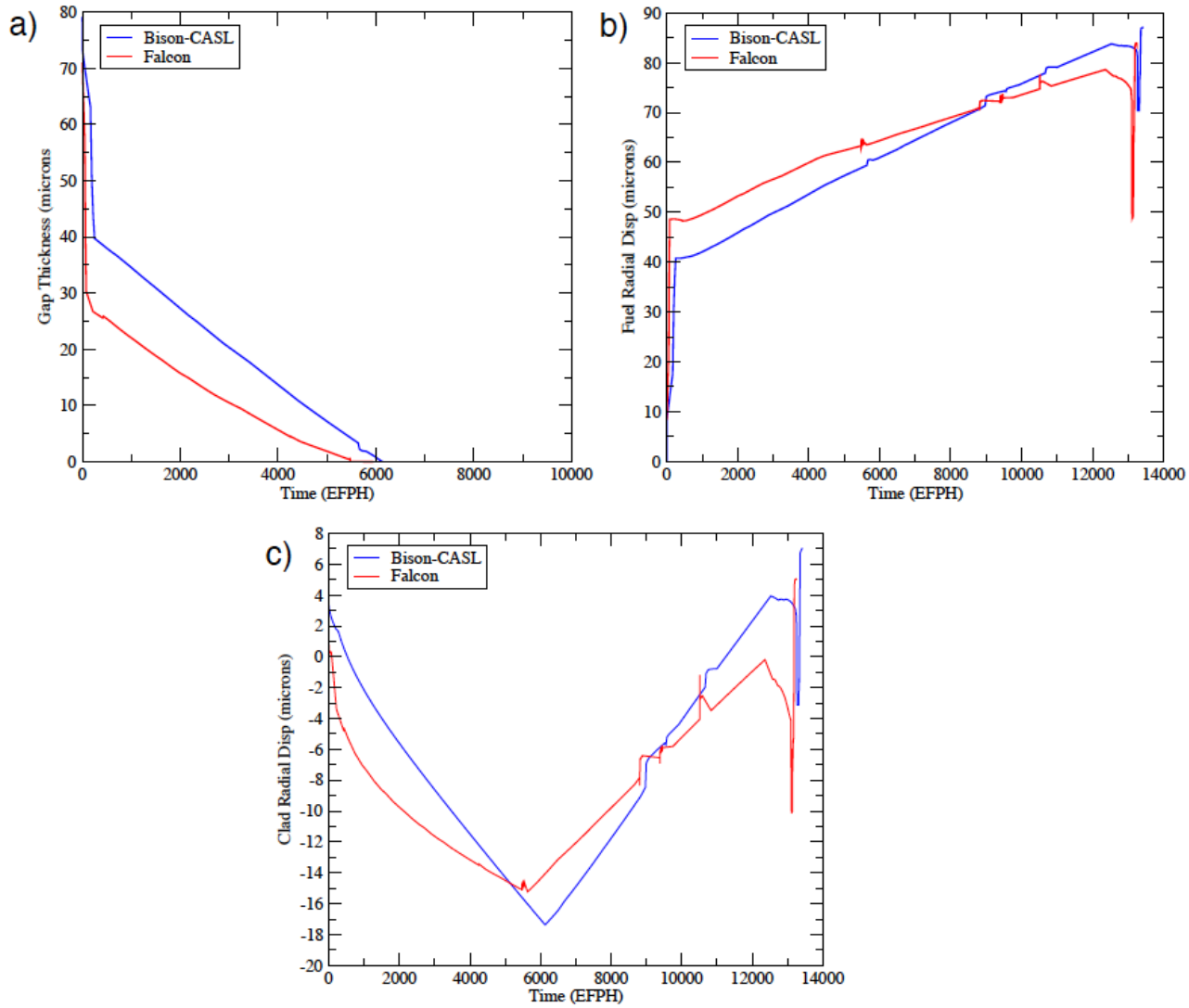

Figure 13. Comparison of BISON-CASL and FALCON fuel performance simulations during cycle 10 and the startup of cycle 11 of the commercial reactor. (a) gap thickness as a function of effective full power hours, (b) fuel radial expansion as a function of effective full power hours, and (c) cladding radial displacement as a function of effective full power hours.

As shown in Fig. 13a), BISON-CASL under predicts relative to Falcon the pellet-cladding gap for the length of the simulations. There are a number of differences between the two codes that affect the results. The first being simulation boundary conditions. As stated earlier, BISON-CASL does not assume any pressure acting on the top or bottom of the cladding, where as Falcon assumes a plenum spring, plenum pressure, and coolant pressure to be acting on the cladding. With Falcon modeling the force of the spring it would be expected for Falcon to have less initial radial expansion than BISON-CASL. As the power begins to increase Falcon calculates a smaller gap when compared to BISON-CASL, seen in Fig. 13b). This is contributed to smeared cracking. BISON-CASL does not include smeared cracking, with the reason being that fuel creep is turned off, where as Falcon does. Smeared cracking allows for more fuel expansion based internal stresses causing the fuel to crack. Another difference between Falcon and BISON-CASL is the fission product swelling model. BISON-CASL uses a MATPRO model, which assumes a faster swelling rate than the Falcon model. Lastly, the BISON-CASL simulation does not have an IFBA model to account for He release during

irradiation. IFBA rods contain a burnable absorber, ZrB_2, as a coating on the outer fuel surface to absorb thermal neutrons. Following neutron absorption, boron undergoes alpha decay, thereby producing helium, which over time will contribute to an increase in the plenum pressure. The increase in plenum pressure will affect the expansion in the cladding creating a slightly larger pellet-cladding gap.

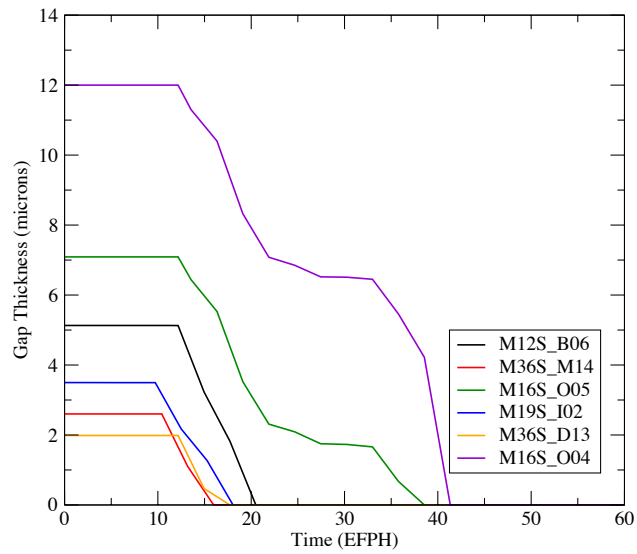

Figure 14. Gap thickness for both the failed and non-failed fuel rods during the commercial reactor cycle 11 startup, as predicted by a 2D R-Z BISON-CASL model.

Table 7. Summary of the 2-D PCI and MPS peak stress and SED analysis.

	Rod Avg Burnup (MWd/tU)	R-Z Peak Stress	PCI Peak Stress	PCI SED	60mil Peak Stress	60mil SED	125mil Peak Stress	125mil SED
M16S_O05 (F)	20.7	77	335	.894	537	1.67	685	4.76
M16S_O04 (NF)	19.6	14	274	.613	459	1.22		
M12S_B06 (F)	33.24	103	421	1.36	629	2.29		
M19S_I02 (F)	31.6	109	414	1.32	622	2.24		
M36S_D13 (NF)	25.5	153	463	1.63	687	2.72		
M36S_M14 (NF)	29.3	140	458	1.6	668	2.59		

F – Rod that failed

NF – Rod that did not fail

Figure 14 compares the hot zero power gap along with the response to an increase in power. Fig. 14 clearly indicates that the rods that experienced the highest nodal burnup have the smallest fuel-clad gaps. As the nodal burnup increases, the fuel expands more and the cladding creeps down more, resulting in a smaller gap. For the two rods within a single assembly, M16S_O04 and M16S_O05,

the pellet-cladding gap remained open for the duration of cycle 10. However during the cycle 11 startup, all rods closed the gap. The results from Figure 14 further provide confidence in our R-Z simulations and correspondingly, provide the initial conditions need for a more detailed failure assessment in 3D. Table 7 provides a summary from the 2-D PCI analysis, including for rod M16S_O04 which contained a MPS of varying size.

Table 7 further validates the results shown in Figure 14. In all cases, the 2D R-Z model results presented in Table 7 indicate that the fuel rods with higher rod average burnup generally have higher maximum clad hoop stress values. However, the highest hoop stresses are predicted for the M36S rods, which do not have the highest rod average burnup and that did not experience fuel failures. The fuel rods in the M36S assembly were operated with an aggressive axial profile, meaning that the axial burnup values varied substantially. With the peak stress being located at a nodal location exposed to higher powers for long periods of times, it would have accumulated a much higher burnup as compared to the rest of the rod resulting in a smaller local gap.

Conducting the same PCI analysis as performed in Section 4, yields a similar result for the R-Z analysis. The presence of radial crack(s) increases the hoop stress on the inner surface of the cladding. When referring back to Figure 9 of Section 4, fuel rods began to fail around stresses of ~450 MPa and a SED of ~1.5 MJ, which are comparable to the values obtained in the analysis performed by Lyon and co-workers [20]. However, when using these values as a potential threshold failure value for the commercial fuel rods shown in Table 7, it is not possible to explain why rods M19S_I02, M16S_O05, and M12S_B06 failed. The stress and SED values for the M16S_O05 fuel rod clearly fall below the failure threshold values, and therefore, this 2D analysis rules out classical PCI as a failure mechanism. M19S_I02 and M12S_B06 both have peak stresses and SEDs comparable to those seen in failed rods in Figure 9, and thus it is possible that classical PCI could have been the responsible failure mechanism in these two rods. Again, however, the M36S rods have higher stress levels and higher SEDs than rods M12S_B06 and M19S_I02, which provides some evidence against classical PCI as the failure mechanism. Correspondingly, we have analyzed several of these rods with MPS defects to assess whether an MPS is the cause of fuel cladding failure.

Table 7 also documents the calculated stress and strain energy density when MPS, with a dimension of 60 mils is present in the fuel rods. As anticipated, the presence of a MPS significantly increased the calculated cladding hoop stresses. When comparing the two fuel rods, M16S_O04 and M16S_O05, which had similar burnups and gap thickness due to being companion rods in the assembly, the failed rod M16S_O05 has consistently higher stresses than the non-failed rod M16S_O04. The maximum clad hoop stress is plotted in Figure 15 for these two rods for the various analysis assumptions summarized in Table 7. This 2D MPS analysis appears to confirm the conclusion that the presence of a MPS is needed for rod M16S_O05 to reach sufficiently high hoop stress to initiate failure, and lends credence to the assumption that a MPS potential could have been present in the failed rods M12S_B06 and M19S_I02. The PIE examination of rod M16S_O05 [7] clearly identified the presence of a large MPS, which had a width of ~125mil and a length of ~3/4 pellet length at the failure location [7]. By incorporating a 125mil MPS in the 2D BISON-CASL simulation, the maximum hoop stress in the clad is increased to 685 MPa, also shown in Figure 15. This validates the conclusion that MPS was the cause of failure in rod M16S_O05.

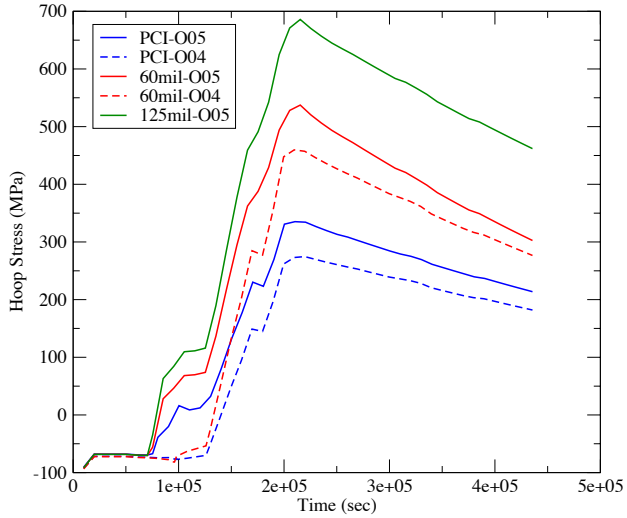

Figure 15. Predicted maximum hoop stress in the clad for fuel rods M16S_O05 and M16S_O04 during cycle 11 startup for various analysis assumptions.

Table 8 summarizes similar analysis data as that of Table 7, however, the results in Table 8 come from a full 3D modeling analysis for PCI and MPS defects. The same general trends hold for the 3D analysis as the 2D results, however. The results of Table 8 should also be considered with respect to the 3D modeling of the ramp test results presented in Figure 10 of Section 4. That analysis indicated that appropriate failure probabilities should be considered as a critical value of ~350 MPa for stresses and 1 MJ for SED. A comparison to the results presented in Table 8 again indicate that classical PCI can not be the cause of failure in rod M16S_O05, but potentially could have been the underlying cause of failure in rods M19S_I02 and M12S_B06. Further evaluation of the presence of the MPS defect reinforces the conclusion that the MPS is the root cause for the cladding failures.

Table 8. Summary of the 3-D PCI and MPS peak stress and SED analysis for the commercial reactor fuel rods.

	Burnup (MWd/tU)	R-Z Peak Stress	PCI Peak Stress	PCI SED	60mil Peak Stress	60mil SED	125mil Peak Stress	125mil SED
M16S_O05 (F)	20.7	77	262	.52	391	1.01	526	1.7
M16S_O04 (NF)	19.6	14	173	.249	314	.723		
M12S_B06 (F)	332.4	103	336	.851	466	1.41		
M19S_I02 (F)	31.6	109	327	.779	461	1.38		
M36S_D13 (NF)	25.5	153	N/A	N/A	547	1.88		
M36S_M14 (NF)	29.3	140	378	1.02	531	1.8		

F – Rod that failed

NF – Rod that did not fail

Evaluating power ramp rate restrictions

It is commonly believed that reducing cladding failure resulting from PCI to 0% can not be accomplished by assuring manufacturing quality alone. The analysis of fuel failures in a commercial reactor performed in this study is a clear example. Westinghouse uses a fuel quality assurance that does not allow a MPS of 60mils wide and 60mils in length to be loaded into a PWR [29]. This is an example where it is possible that the quality assurance broke down since the resulting MPS dimensions determined by post-irradiation examination clearly indicated an MPS length of 125 mils. Another possible approach to limiting PCI fuel failures is to limit the power ramp levels.

Figure 16 and Table 9 illustrate the results of our BISON-CASL modeling assessment of utilizing reduced ramp rates to reach peak linear power to reduce clad stress levels. The first method attempts to slow the ramp to full power by one-half, one-third and one-fourth of the original power ramp rate. For the power ramp and hold times in the current analysis, there is almost no affect seen by increasing the amount of time to reach full power. By continuing to increase the power, the fuel is constantly expanding radially and not allowing sufficient time for the cladding stresses to relax. However, the implementation of a constant power hold time during the power ramp can significantly reduce the cladding stresses. Fig. 16a demonstrates the hold time at a power level of 80% of the maximum value. Fig. 16b indicates that during this step power ramp, the clad hoop stress is able to significantly decrease, and that the resulting peak stress upon finally reaching full power is also substantially less than during a continual power increase. While this is a relatively simple test case to evaluate power ramp rate effects on the maximum clad stress, it does indicate that there are operational approaches to minimize the potential for cladding failure.

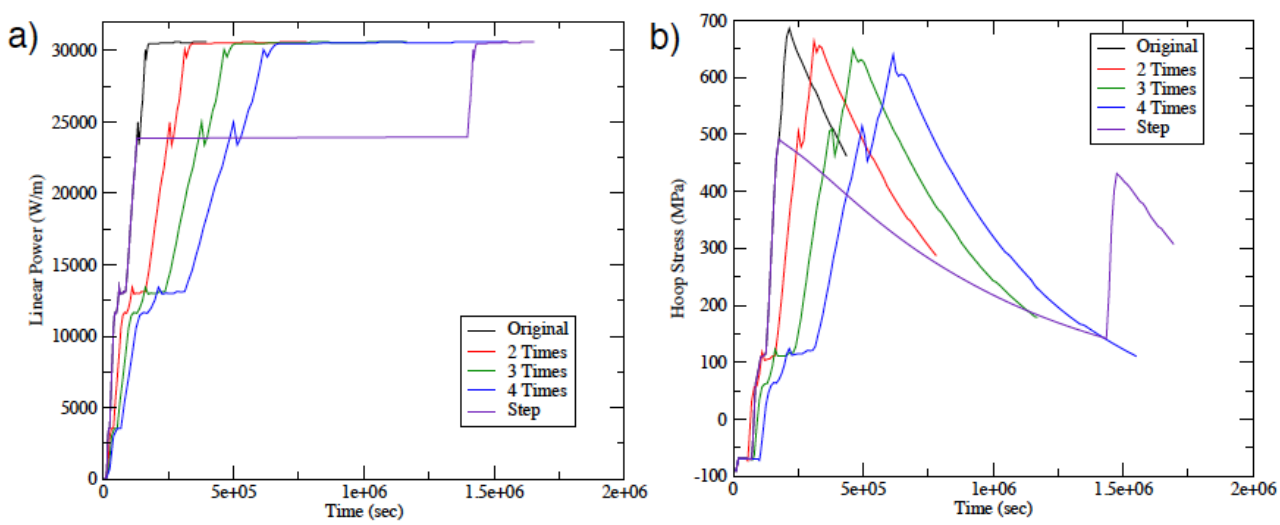

Figure 16. a) Modified power histories and b) corresponding peak clad stresses during power ramp startup of cycle 11 for the fuel rod M16S_O05.

Table 9. Peak stress and SED values from the ramp study, shown in Fig. 16a.

	Peak Stress (MPa)	Peak SED (MJ)
Classical PCI	251	4.76
Original Power History	685	6.85
2 Times Original	655	2.45
3 Times Original	648	2.4
4 Times Original	640	2.3
Step Added	491	1.36

Evaluating uncertainty in power profiles

Power histories, material properties, as well as experimental cladding and fuel displacements have inherent uncertainties. It has been shown that rod average power histories can have anywhere from 3-5% and as much as 10% uncertainty associated with the measured power [30]. To evaluate the impact that uncertainties in the measured power may have on predicted clad stress and failure probability, we have performed an initial statistical evaluation of the impact on variations in the power history. Figure 17 evaluates the statistical uncertainties present in the measured power history, by reducing the power by 3-5% for rod M16S_O05 (failed) as well as by increasing the power by 3-5% for rod M16S_O04 (non-failed). Again, these rods were in the same assembly and operated under similar power conditions. The biggest difference between these two rods was M16S_O05 failed, due to the presence of a MPS.

Fig. 17 indicates that there is a relatively small change in the hoop stress when the power is adjusted from 3-5%. But, when comparing the stress produced in rod O05 versus O04 by a 5% decrease or increase, respectively to the power history, this results in a ~25 MPa change in cladding hoop stress. This change in cladding stress is verified when comparing various pellet defects, e.g classical PCI and MPS, as shown in Figure 18. The analysis performed for Fig. 18 uses the M16S_O05 geometry, and compares peak stresses produced by radial cracks and two different MPS widths. For each change (reduction in power history), there is a slight decrease in the peak cladding hoop stress. Figure 18 shows that a 5% change in power, either increase or decrease, can be expected to have an ~20MPa impact on the peak cladding hoop stress. Using a peak stress failure criteria model, this increase or decrease in cladding stress would be insignificant. However, more advanced crack evolution models may not consider this an insignificant increase in stress. Assuming a traditional mode 1 fracture toughness model, a full fracture mechanics analysis would indicate a stress concentration effect of about a factor of three times the applied stress near a crack tip. That means that an applied hoop stress increase of 20 MPa could result in a local stress at the crack tip which is higher by 60 MPa. It is unclear how this increase will affect the failure potential however, the results show how uncertainties in the power history can increase the cladding failure potential.

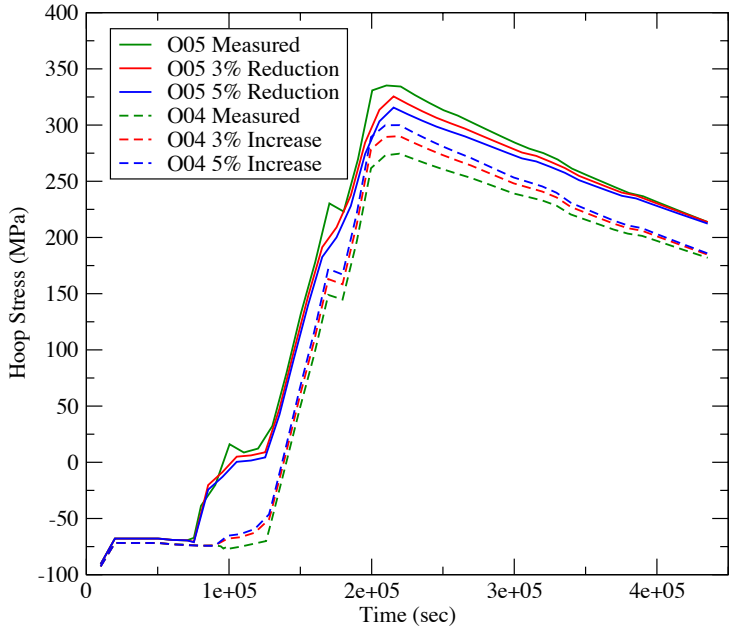

Figure 17. Predictions of the clad hoop stress for fuel rods M16S_O04 and M16S_O05, based on 3-5% variations in the power history during cycle 11 startup.

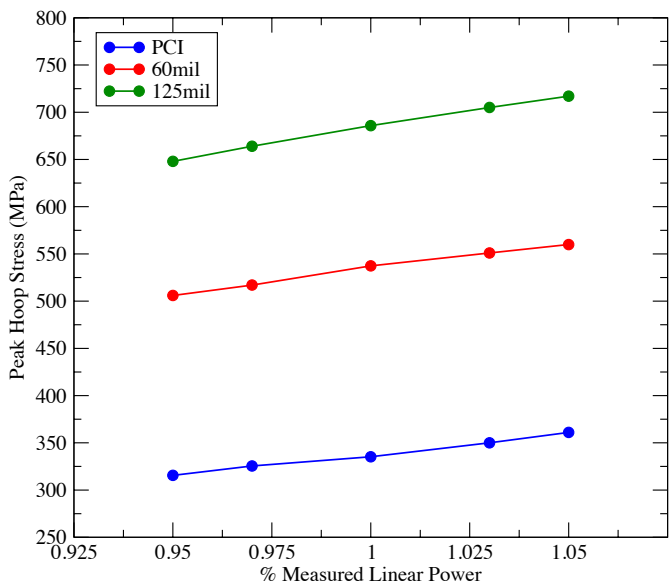

Figure 18. Evaluation of the peak clad stress in fuel rod M16S_O05 during cycle 11 startup, with variations in the linear power between ±5% based on analysis assumptions including a 60 mil or 125 mil MPS defect.

5. CONCLUSIONS AND FUTURE WORK

The FY15 milestone activities associated with BISON-CASL fuel performance modeling was to present and evaluate a methodology for fuel failure assessment and to assess the modeling predictions against actual commercial power reactor fuel failure experience. Data from a set of PWR ramp test rods taken from the IFPE database were used to evaluate both the maximum hoop stress in the fuel clad, as well as the cladding SED, as possible failure assessment methodologies applicable to the PCI/MPS fuel failure mechanism. Secondly, this report summarizes the BISON-CASL modeling results for fuel failures observed in a commercial nuclear

power plant during the power ramp increase associated with startup during cycle 11 of that reactor's operation. The objectives of these analysis were to 1) evaluate the cladding hoop stress conditions at the suspected time of cladding failure to assess the potential role of PCI in the failure process, 2) provide a PCI fuel failure assessment to determine if the presence of a MPS was required for cladding failure to occur, and 3) demonstrate a reactor startup recommendations to minimize the potential for PCI related cladding failure.

The results of the BISON-CASL fuel performance modeling in 2D (R-Z or R-θ) are broadly consistent with current industry code capabilities, and the 3D modeling capability clearly provides a unique capability to industry. As with other assessments performed previously [7,9,20], the evaluation of fuel failure data from test reactor ramp tests indicates that the maximum hoop stress and SED based criteria will not adequately isolate failed rods from non-failed rods. Further, these methods are quite statistically sensitive to the assumptions used in the hoop stress and SED calculations. It appears that as a metric, neither the peak cladding hoop stress nor the SED alone, is sufficient to define rod failure. As a result, implementation of the failure probability thresholds defined by stress or SED could over conservatively restrict reactor operation.

The fuel history from several fuel rods from a commercial reactor during operation in cycle 10 and startup to cycle 11 were used to evaluate the overall fidelity of the BISON-CASL fuel performance modeling. The BISON-CASL analysis demonstrated that both cladding hoop stress and SED increased significantly during the startup ramp between cycle 10 and the startup to cycle 11. The increase in these two possible failure indicators was caused by pellet-cladding mechanical interaction as a result of the fast startup ramp rate and the axial flux change. The BISON-CASL analysis in both 2D and 3D clearly indicated that the presence of a MPS was the cause for fuel rod M16S_O05 to have failed. Rods M19S_I02 and M12S_B06 both showed higher PCI stress values and thus it is possible that the failure of these rods was caused by either an MPS or possibly by some other mechanism, including a cladding corrosion assisted failure process. Lastly, a demonstration of reactor startup power ramps has shown one possible power hold and ramp combination that has the ability to significantly reduce the maximum clad hoop stress and presumably minimize the potential for PCI related cladding failure. The potential for classical PCI based failures for higher burnup fuel than the rods analyzed in the current study remains for future consideration.

While this assessment demonstrates that BISON-CASL is evolving into a robust capability to provide mechanistic modeling and understanding for assessing PCI failure potential, several areas of further work and improvement were noted, including: 1) continuing to develop a robust 3-D contact algorithm utilizing less memory and better convergence success at high contact pressures; 2) a more robust smeared cracking model, which gives the ability to implicitly represent the fracture behavior of the ceramic UO_2 pellet to calculate crack formation, extension, and pellet mechanical compliance; 3) developing a relocation model that is informed based on the pellet-cladding gap; and 4) interfacing with a mechanistic model to assess stress corrosion cracking and crack propagation in the fuel clad. Future BISON-CASL development activities will be needed to implement advanced mechanistic models which we expect to further increase the predictive nature of the CASL fuel performance modeling.

Finally, establishing the fuel rod conditions prior to a power maneuver remains a critical element to modeling the potential for PCI failure. Further work on BISON-CASL will focus on integrating micro-scale models under development in CASL-FMC that describe the irradiation creep and growth of zirconium alloys, the fracture, relocation, and mechanical compliance of the fuel pellet, and the release of fission products important for SCC (volatile and noble gases). The incorporation of these models into BISON-CASL, either directly or using improved semi-empirical relationships, will require expanding the validation activities of BISON-CASL to include more integral fuel rod irradiations, hot-cell examination data from commercial reactor fuel rods, and separate effects experiments.

6. REFERENCES

1. B. Cox, Pellet Cladding Interaction (PCI) Failures of Zirconium Alloy Fuel Cladding – A Review, Journal of Nuclear Materials, 172 (1990) 249-292
2. M. F. Lyons, D. H. Coplin and C. G. Jones, GE Quarterly Progress Reports, GEAP - 3771-10 to -12 (1963/64)
3. J.T.A. Roberts and F.E. Gelhaus, "Zircaloy Performance in Light Water Reactors," Zirconium in the Nuclear Industry (Fourth Conference), ASTM STP 681, ASTM, 1979, pp. 19-39
4. F. Garzarolli, R. von Jan, H. Stehle, The Main Causes of Fuel Element Failure in Water-Cooled Power Reactors, Atomic Energy Review, **17**, 1 (1979)
5. R. O. Montgomery et al, "Peregrine: Validation and Benchmark Evaluation of Integrated Fuel Performance Modeling Using Test Reactor Data and Falcon," L1.CASL.P7.02, June, 2013.
6. N. Capps, R. Montgomery, D. Sunderland, M. Pytel, and B.D. Wirth, "Evaluation of Missing Pellet Surface Geometry on Cladding Stress Distribution and Magnitude", *Nuclear Engineering and Design* (2015) under review.
7. Y. Aleshin, C. Beard, G. Mangham, D. Mitchell, E. Malek, and M. Young, "The Effect of Pellet and Local Power Variations on PCI Margin", Proceedings of Top Fuel 2010, September 26-29, 2010, Orlando, FL, USA, Paper 041.
8. Corie Glenn and Tyrone L. Stevens, Exelon Corp., personal communication (2015).
9. EPRI Report 1012915, "PCI Analyses and Startup Ramp Rate Recommendations for Westinghouse Fuel in Exelon PWRs", (2006).
10. D. Gaston, C. Newman, G. Hansen, and D. Lebrun-Grandie, "MOOSE: parallel computational framework for coupled systems of nonlinear equations. Nucl. Eng. Design," 239, p. 1768–1778, 209.
11. R. Williamson, J. Hales, S. Novascone, M. Tonks, D. Gaston, C. Permann, D. Andrs, and R. Martineau, "Multidimensional multiphysics simulation of nuclear fuel behavior," *Journal of Nuclear Materials* 423 (2012) 149–163.
12. R. Montgomery, et al., "Peregrine: Advanced Modeling of Pellet-Cladding Interaction (PCI) Failure in LWRs," Proceedings of the TopFuel 2012 Reactor Fuel Performance Conference, Manchester, United Kingdom, September 2-6, 2012.
13. B. W. Spencer, J. D. Hales, D. R. Gaston, D. A. Karpeev, R. L. Williamson, S. R. Novascone, D. M. Perez, R. J. Gardner, and K. A. Gamble. BISON contact improvements CASL FY14 report. Technical Report INL/EXT-14-33285, Idaho National Laboratory, Idaho Falls, ID, September 2014.
14. D. S. Stafford and B.W. Spencer. Contact memory reduction CASL letter report. Technical report, Idaho National Laboratory, Idaho Falls, ID, January 2015.
15. SIERRA Solid Mechanics Team. Sierra/SolidMechanics 4.22 user's guide. Technical Report SAND2011-7597, Sandia National Laboratories, Albuquerque, NM, October 2011.
16. S. Djurle, "Final Report of the Super-Ramp Project," STUDSVIK-STSR-32, Dec. 1984.
17. S. Djurle, "Final Report of the Over-Ramp Project," STUDSVIK-STSR-37, Dec. 1980.
18. Turnbull, J.A.; Studsvik Nuclear AB, SE-611 82 Nykoeping (Sweden).
19. Turnbull, J.A.; CEA - Dept. des Reacteurs Nucleaires, 91191 Gif-sur-Yvette Cedex (France).
20. W. Lyon, R. Montgomery, Y. Rashid, "PCI Analysis and Fuel Rod Failure Prediction using FALCON," Proc. TOP FUEL '09, Paris, France, 2009.
21. Westinghouse Letter PPE-05-159, "Generic Data Requirements for PCI Analysis," dated July 7, 2005.

22. Westinghouse Letter PCT-05-542, “Rod Power history Data for transmittal to ANATECH,” July 1, 2005.
23. Westinghouse Letter PPT-05-54, “ANC Identification of Failed Rods in Braidwood Unit 1,” July 5, 2005
24. Westinghouse Letter PCT-05-556, “Rod Power history Data for transmittal to ANATECH,” July 14, 2005
25. Sabol, G. P., Comstock, R. J., Weiner, R. A., Larouere, P., and Stanutz, R. N., “ In-Reactor Corrosion Performance of ZIRLO and Zircaloy-4,” Zirconium in the Nuclear Industry: Tenth International Symposium, ASTM STP 1245, A. M Garde and E.R. Bradley, Eds.. American Society for Testing and Materials, Philadelphia, 1994. p 724-744.
26. QUECEDO et al., Results of Thermal Creep Test on Highly Irradiated ZIRLO
27. C.-S. Seok et al. / Engineering Failure Analysis 13 (2006) 389–397
28. C.S. Seok et al. / Nuclear Engineering and Design *241 (2011) 599–602*
29. Shah, Hemant, Aleshin, Yuriy, Sutharshan, Balendra ., Borell, Sten, & Widegren, Hans (2007). Enhanced fuel performance by improving pellet quality and fabrication technology. *Proceedings of the ICONE-15 (Revised) The 15th international conference on nuclear engineering,* (p. 3174). Japan: Japan Society of Mechanical Engineers.
30. S. Palmtag, CASL, personal communication (2015).